

JARO 14: 523–545 (2013)

DOI: 10.1007/s10162-013-0393-0

© 2013 The Author(s). This article is published with open access at Springerlink.com



JARO
Journal of the Association for Research in Otolaryngology

Research Article

The Spatial Buildup of Compression and Suppression in the Mammalian Cochlea

CORSTIAEN P. C. VERSTEEGH¹ AND MARCEL VAN DER HEIJDEN¹¹*Department of Neuroscience, Erasmus MC, P.O. Box 20403000 Rotterdam, The Netherlands*

Received: 18 January 2013; Accepted: 23 April 2013; Online publication: 21 May 2013

ABSTRACT

We recorded responses of the gerbil basilar membrane (BM) to wideband tone complexes. The intensity of one component was varied and the effects on the amplitude and phase of the others were assessed. This suppression paradigm enabled us to vary probe frequency and suppressor frequency independently, allowing the use of simple scaling arguments to analyze the spatial buildup of the nonlinear interaction between traveling waves. Most suppressors had the same effects on probe amplitude and phase as did wideband intensity increments. The main exception were suppressors above the characteristic frequency (CF) of the recording location, for which the frequency range of most affected probes was not constant, but shifted upward with suppressor frequency. BM displacement reliably predicted the effectiveness of low-side suppressors, but not high-side suppressors. We found “anti-suppression” of probes well below CF, i.e., suppressor-induced enhancement of probe response amplitude. Large (>1 cycle) phase effects occurred for above-CF probes. Phase shifts varied nonmonotonically, but systematically, with suppressor level, probe frequency, and suppressor frequency, reconciling apparent discrepancies in the literature. The analysis of spatial buildup revealed an accumulation of local effects on the propagation of the traveling wave, with larger BM displacement reducing the local forward gain. The propagation speed of the wave was also affected. With larger BM displacement, the basal portion of the wave slowed down, while the apical part sped up. This framework of spatial buildup of local effects unifies

the widely different effects of overall intensity, low-side suppressors, and high-side suppressors on BM responses.

Keywords: cochlear mechanics, laser interferometry, dynamic range compression, two-tone suppression, basilar membrane, traveling waves

INTRODUCTION

The nonlinear processing of sound in the auditory periphery often produces strong interactions between stimulus components. Such interactions have been extensively studied in the responses of auditory nerve (AN) fibers to tone pairs. The response to a probe tone at a fiber’s characteristic frequency (CF) can often be reduced (or even completely suppressed) by adding a second tone (suppressor) at a different frequency (Sachs and Kiang 1968). Two-tone suppression is tightly linked to auditory masking (Delgutte 1990). Suppression has also been observed in basilar membrane (BM) responses (reviewed in Robles and Ruggero (2001)) and although there is incomplete consistency between AN and BM data, the similarities suggest that cochlear mechanical nonlinearity is the major source of suppression in the AN (Ruggero et al. 1992; Cheatham 2008). Apart from its relation to neural suppression and perceptual masking, suppression in BM responses is an interesting subject by itself, because it provides a powerful and sensitive tool for the study of cochlear nonlinearity. Suppression in BM responses is a direct consequence of the dynamic range compression of the cochlea, i.e., the adjustment of mechanical sensitivity to the stimulus intensity (Cooper 2004), and one can even view the compressive growth of single-tone BM responses as a form of “self-suppression” (Kanis and De Boer 1993).

Correspondence to: Marcel van der Heijden · Department of Neuroscience · Erasmus MC · P.O. Box 20403000 Rotterdam, The Netherlands. Telephone: +31 (0)10 7043558; fax: +31 (0)10 7043462; URL: <http://beta.neuro.nl/research/vanderheijden>

From a functional point of view, compression is needed to map the dynamic range of sounds to the more limited dynamic range of transduction channels and AN fibers. Ideally, dynamic range compression should not interfere with the other major task of the cochlea, spectral analysis. A simple wideband gain control does not meet this requirement, as it would allow any strong stimulus component to “shut down” the entire cochlea. The best strategy is to provide independent compression in each frequency band. Such multiband compression is easily realized in a filter bank, where different frequency bands are processed along independent, parallel paths. The cochlea, however, is a waveguide in which the different frequency components travel along a single path. The overlap is likely to frustrate the independence of the frequency bands at some point. Nevertheless, the cochlea appears to closely approach multiband compression for low and moderate intensities. For higher intensities, the frequency selectivity of compression breaks down asymmetrically, with low frequencies suppressing high frequencies more easily than conversely (“upward spread of masking,” Wegel and Lane 1924).

The spectral asymmetry is a direct consequence of the traveling wave character of cochlear processing, in which low-frequency waves traverse the high-frequency end of the cochlea, while high-frequency waves never reach the low-frequency region of the cochlea because they rapidly decay after reaching their characteristic place. The asymmetry pervades the data on suppression, creating a number of differences between low-side suppression (suppressor frequency below probe frequency) and high-side suppression (Ruggero et al. 1992; Rhode and Cooper 1993; Rhode and Recio 2001b). The most salient difference is the growth of suppression with suppressor intensity, which is much steeper for low-side suppressors than for high-side suppressors.

Besides reducing the amplitude of probe responses, suppressors also affect their phase (reviewed in Robles and Ruggero (2001)). Both phase leads and lags have been observed, depending on suppressor frequency, probe frequency, and suppressor intensity. The shifts are often nonmonotonic: leads turn into lags with increasing suppressor intensity. When using CF probes (the most common choice), phase shifts usually do not exceed 0.25 cycle, but off-CF probes can yield phase shifts as large as 0.5 cycle (Rhode 2007b).

The interpretation of these complex phenomena is challenging. It would be helpful if one could record the motion of the BM along the entire path of the traveling waves of probe and suppressor, and study how their nonlinear interaction develops as they propagate. The anatomy and vulnerability of the cochlea prevents such a panoramic approach. Fortunately, the tonotopic map of the cochlea provides an alternative approach, in which variations in stimulus

frequency are used as a proxy for multilocation recordings. This tradeoff or “scaling” (Zweig 1976) is not exact (Ren 2002; Shera 2007), but provides a useful tool for the analysis of BM data. A systematic analysis of suppression along these lines requires a body of data in which the frequencies of probe and suppressor are independently varied. The main goal of this study was to provide such data. Most previous cochlear mechanical studies on suppression used a wide range of suppressor frequencies and only a limited range of probe frequencies near CF (Ruggero et al. 1992; Rhode and Cooper 1993; Cooper 1996; Geisler and Nuttall 1997; Rhode and Recio 2001b). Several studies used tone complexes (two to seven components) and found mutual suppression among the components (Rhode and Recio 2001a, b). Rhode (2007b) used a wide range of probe frequencies for a fixed CF suppressor and vice versa. He also found mutual (but asymmetric) suppression across the tone pairs.

We used irregularly spaced wideband tone complexes consisting of 40 tones and kept the levels of all tones except one (the suppressor) constant at 20 dB SPL. The suppressor intensity was systematically varied; the remaining 39 components served as probes. This paradigm allowed us to study the effect of probe frequency more systematically and extensively than in previous studies. In particular, it enabled us to vary probe frequency and suppressor frequency independently. In the first stage of analysis, we addressed the following questions.

- Does the equivalence of suppression and compression (Cooper 1996) hold for the wider range of probe frequencies?
- Do high-side and low-side suppression really have identical frequency tuning (i.e., dependence on suppressor frequency), as found for a limited frequency range by Ruggero et al. (1992)?
- When using CF probes, BM displacement is a good predictor of low-side suppression (Cooper 1996; Geisler and Nuttall 1997). Does this generalize to off-CF probes?
- Phase shifts in two-tone suppression can be considerably larger than intensity-induced phase shifts in single-tone responses (Rhode 2007b). Are there specific probe/suppressor combinations that produce particularly large effects?
- How do the nonmonotonic phase effects of suppression (Cooper 1996; Rhode and Recio 2001b; Rhode 2007b) fit into the larger test space?

These questions were answered by straightforward analyses of the data.

In the second analysis stage, we used scaling arguments to characterize the local interaction of traveling waves that produces suppression and com-

pression. This analysis revealed that many seemingly unrelated aspects of compression and suppression are in fact consequences of the gradual accumulation of suppression along the travel direction. Likewise, the complex phase effects were found to reflect systematic changes in the local propagation speed of traveling waves.

MATERIALS AND METHODS

Animal preparation

We recorded stapes and BM motion from single locations in five cochleae of Mongolian gerbil (*Meriones unguiculatus*; female, ~60 g) with CFs of 13.4–22.5 kHz. A detailed description of the surgical approach is found in Versteegh and Van der Heijden (2012). In short, the animal was anesthetized and the pinna removed. The bulla was opened, granting a clear view of the round window. The round window membrane was torn and reflective beads (silver-coated hollow-glass microspheres, 25 μm , 1.0–1.2 g/cm³; Nanoparticulate Surface Adhesion Ltd., Loanhead, UK) were allowed to settle on the BM. The air–fluid interface was stabilized by placing a glass cover slip over the round window. All procedures were approved by the Erasmus MC Laboratory Animal Committee.

Recording system

Stimuli generated by a personal computer with custom MATLAB-software (The MathWorks, Natick, MA, USA) were fed through a 24-bit D/A-channel (RX6; Tucker-Davis Technologies (TDT), Alachua, FL, USA) at 111.6 kHz. A programmable attenuator (PA5; TDT) followed by an amplifier (SA1; TDT) conditioned the signal before a speaker (CF1; TDT) played the stimuli. The speaker was connected to a sound delivery probe sealed to the ear canal with Vaseline. The sound system varied less than 4 dB in the 5–25 kHz range after correcting for the acoustic transfer of the probe.

We measured a bead's velocity with a single-point laser vibrometer (OFV-534; Polytec, Waldbronn, Germany) through an illumination unit (VIB-A-510; Polytec) and a 5 \times or 10 \times microscope objective (M Plan Apo 5 \times , NA=0.14, $f=40$; M Plan Apo 10 \times , NA=0.28, $f=20$; Mitutoyo, Veenendaal, The Netherlands). The output signal was fed to a velocity decoder (VD-06; Polytec) and was sampled by a 24-bit A/D-converter (RX6; TDT) at 111.6 kHz before being stored on hard disk. Recordings of BM motion were corrected for the 0.75-fold reduction of the speed of light in water compared to air. All experiments were carried out in a double-walled sound-isolating booth (Acoustair, Moerkapelle, The

Netherlands) and on an optical table (Newport, Irvine, CA, USA).

Stimuli and analysis

The broadband stimuli were essentially those detailed in Versteegh and Van der Heijden (2012), now coming in two forms: the equal-amplitude stimuli used in that study and novel ones with one (suppressor) component elevated. In short, the stimuli consisted of 40 frequency components in the 0.1–30 kHz range (experiments RG12408, RG12449) or 0.1–25 kHz range (experiments RG12411, RG12420, and RG12421). These components were irregularly spaced, making sure that combination tones up to the third order did not coincide with any of the 40 primary components. The same set of components and random starting phases was used within one experiment, but this set varied across experiments. A single stimulus lasted ~15.05 s. The intensity of the equal-amplitude stimulus ranged from 0 to 80 dB SPL (experiments RG12411, RG12420, and RG12421) and from 0 to 76 dB SPL (experiments RG12408 and RG12449) per component and was increased in 10-dB steps (the final step was 6 dB in the latter two experiments). When playing the multitone stimulus at 80 dB SPL per tone, acoustic distortion, measured in a cavity using a 0.25-in. microphone (Brüel and Kjaer, Naerum, Denmark) and evaluated as described in Versteegh and Van der Heijden (2012; see their Fig. 8), was ~46 dB below the stimulus components, independent of frequency in the 0.5–25 kHz range. The CF was determined post hoc as the peak of the unsuppressed 0 dB SPL velocity frequency curve normalized to middle ear motion.

The novel stimulus was almost identical to the 20-dB-SPL equal-amplitude stimulus, the only difference being that the intensity of a single frequency component (the suppressor) was increased, ranging from 30 to 80 dB SPL in 10 dB steps (experiment RG12449 included a 90-dB-SPL suppressor). Components above 12 kHz all served, in turn, as a suppressor. Below 12 kHz, a subset that varied across experiments served as suppressors.

We found that long-term (>5 min) sensitivity reduction with slow recovery occurred both after playing a high-intensity (≥ 70 dB SPL) equal-amplitude stimulus and after playing any stimulus that gave a strongly suppressed response, which usually required the suppressor to have an intensity ≥ 70 dB SPL. To limit the effects of this long-term sensitivity reduction, the order of recording was adjusted in the following way. The experiments started with flat-amplitude recordings of 0, 10, and 20 dB SPL. Next, the first recordings using a single-component suppressor were done, with suppressor intensity $L_{\text{supp}}=30$ dB SPL and in order of descending suppressor frequency.

After these recordings, the 30-dB-SPL equal-amplitude stimulus was used, followed by a 20-dB-SPL equal-amplitude stimulus. Thereafter, single suppressors with $L_{\text{supp}}=40$ dB SPL were tested, again in descending frequency order, followed by the 40-dB-SPL equal-amplitude stimulus and again a 20-dB-SPL equal-amplitude stimulus. This order of stimulus-intensity increments continued until the last 80 dB suppressive stimulus was followed by the highest intensity (76 or 80 dB SPL) equal-amplitude stimulus. Experiment RG12408 had a deviant order: first, 0–40 dB SPL flat-amplitude stimuli; then all stimuli containing a single suppressor and the interleaved 20-dB-SPL equal-amplitude stimuli; then 50–76 dB SPL equal-amplitude stimuli.

We used Fourier analysis to extract magnitude and phase for all frequency components in a single response, and Rayleigh statistics ($p < 0.001$) to remove nonsignificant data points (Versteegh and Van der Heijden 2012). All 20-dB-SPL flat-amplitude responses were used to monitor the state of the cochlea and those responses that did not show any sensitivity reduction were pooled to form a reference curve for the suppression measurements. This pooling of the data increased significance of individual data points, improving both the accuracy and the frequency range over which a reference was available.

At the end of each experiment, the laser was focused on a reflective bead near the stapes footplate (except experiment RG12408 which started with middle ear recordings). Recordings were made for referencing BM responses to the middle ear input. Phase data therefore relate BM motion toward scala vestibuli to inward stapes motion. Stimuli consisted of three series of single tones (700-ms duration including 2-ms rise/fall, presented each 1,000 ms; two repetitions): 0.05–5 kHz in 0.04 octave steps at 80 dB SPL, 5–25 kHz in 0.01 octave steps at 80 dB SPL, and 25–45 kHz in 0.01 octave steps at 65 dB SPL. At high intensities (>80 dB SPL) and stimulus frequencies below 5 kHz, middle-ear muscle contraction can affect the stapes response (Møller 1965; Rosowski et al. 2006). However, we assumed the response to be linear over all frequencies and the most relevant part for suppression lies in the linear region of middle ear motion.

All experiments were carried out in cochleae in good physiological condition (Versteegh and Van der Heijden 2012): for flat-amplitude stimuli, four experiments showed nonlinearly compressive responses near CF down to 0 dB SPL per tone, and one experiment (RG12408) showed compression down to 20 dB SPL. The entire BM-stimulus protocol was carried out within 130 min after tearing the round window. Over this time period, sensitivity loss at CF to a 20-dB-SPL equal-amplitude stimulus was <3 dB. Since the intensity of our stimuli increased to the end of the experiment, this loss is unlikely to have influenced our data.

Rate of suppression. The rate of suppression (ROS) is defined as the increase of suppression per decibel increase of suppressor intensity. The slopes of the amplitude curves of Figure 7 are its graphical representations. For each combination of probe and suppressor frequency, the ROS varied with suppressor intensity. The maximum ROS was usually found for suppressor intensities of 50–80 dB SPL by dividing the reduction of probe amplitude (in decibel) by the increment in suppressor intensity (in decibel) and determining its maximum value. In the range of suppressor intensities considered, the probe response could be fully suppressed, meaning that it was pushed below the noise floor. In those cases, an ROS could not be determined even though it might have yielded the maximum ROS. We therefore required the suppressor intensities of 50–80 dB SPL to have significant probe responses for a maximum ROS value to be defined. This explains the discontinuous lines in Figure 9A, B.

Spatial loss gradients. Estimates of loss gradients were obtained from amplitude change data (Figure 2 and corresponding data from the four other cochlea) by converting probe frequency to position on the gerbil BM (Müller 1996) and, for each curve, fitting a straight line to the five points nearest to the BM position ~ 300 μm basal to the best site (i.e., the BM position corresponding to the CF). This range of BM locations corresponded to the steepest part of the amplitude change versus frequency curves in most cases. Root mean square (RMS) displacement of a single recording was determined by taking the Pythagorean sum of the displacements of all Rayleigh significant response components at the stimulus frequencies.

RESULTS

Amplitude and phase change

Responses to equal-amplitude tone complexes, normalized to stapes motion, are shown in the two upper panels of Figure 1. Intensity was varied from 0 to 80 dB SPL per tone. Throughout this study, the display is restricted to response components that were significantly phase locked to the stimulus ($p < 0.001$, Rayleigh test; see “Materials and methods” section). The data in Figure 1A, B are similar to those of Versteegh and Van der Heijden (2012; Figs. 2C, D and 3C, D). The amplitude curves (Fig. 1A) showed a low-frequency tail, compressive growth with stimulus intensity around CF, and a high-frequency plateau. The associated phase curves (Fig. 1B) showed little variation at low frequencies, an accumulation of phase lag around CF, and a high-frequency plateau. With increasing stimulus intensity, phase curves became shallower.

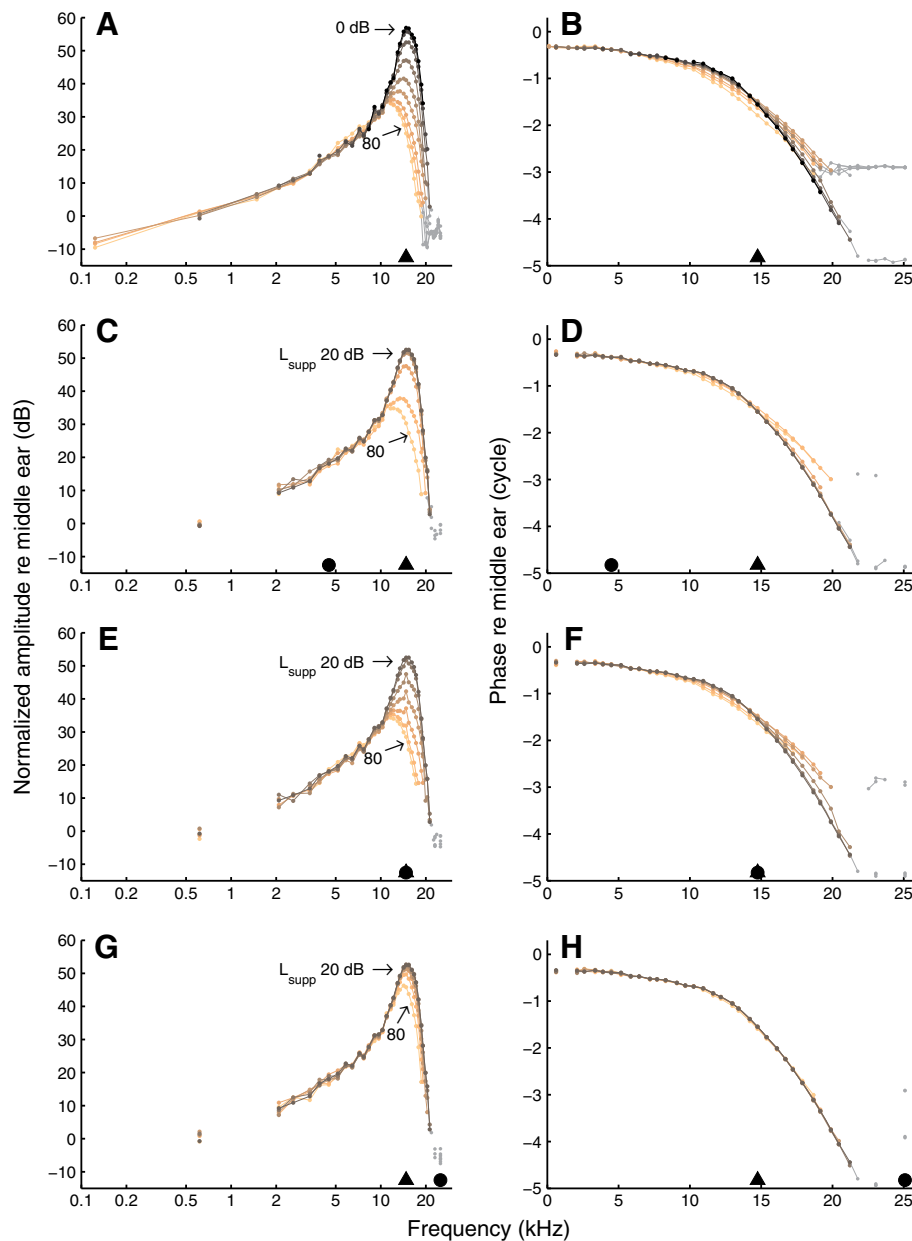


FIG. 1. BM responses to wideband tone complexes. *Left column* amplitude, normalized to stapes motion. *Right column* phase *re* stapes. In **A** and **B**, the intensities of all 40 components of an equal-amplitude complex were varied together in 10-dB steps as indicated in the graph. In the other panels, all components except one (the suppressor) were kept at 20 dB SPL, and suppressor intensity was varied in 10-dB steps as indicated in the graph. *Black triangles* indicate CF (14.8 kHz) and *black circles* indicate suppressor frequency: 4.5 kHz (**C**, **D**), 14.8 kHz (**E**, **F**), and 25.1 kHz (**G**, **H**). Datapoints in the high-frequency plateau are shown in *gray*. Experiment RG12420.

The remainder of the figure (Fig. 1C–H) shows responses to tone complexes in which the intensity of a single tone (the suppressor) was varied, while the 39 other tones (the probes) were kept at 20 dB SPL. The curves having the lowest suppressor intensity (20 dB SPL) are identical to the 20-dB-SPL curves of the upper two panels. Note that even though the suppressor intensity can exceed the probe intensity by as much as 60 dB, the suppressor response components are not elevated owing to the normalization. The data shown in Figure 1C–H were obtained with three different suppressor frequencies f_{supp} (indicated by the *solid black circles*). The effects of the below-CF suppressor on amplitude (Fig. 1C) and phase (Fig. 1D) were similar to the effects of jointly raising the intensities of all tones (Fig. 1A, B). The difference

in spacing of the amplitude curves, however, indicates a higher suppression threshold (i.e., the suppressor intensity needed to reduce the response amplitudes) and a steeper growth of suppression for the below-CF suppressor. These aspects will be analyzed later on. The data obtained with a near-CF suppressor (Fig. 1E, F) were even more similar to the equal-amplitude data (Fig. 1A, B). In contrast, the above-CF suppressor (Fig. 1G, H) produced a different pattern: probes below CF were hardly affected and phase changes were much smaller.

In order to make a quantitative comparison between the different suppressor types, we used the 20 dB-SPL equal-amplitude data as a reference and evaluated probe amplitude and phase effects with respect to this reference (Fig. 2). This display mode

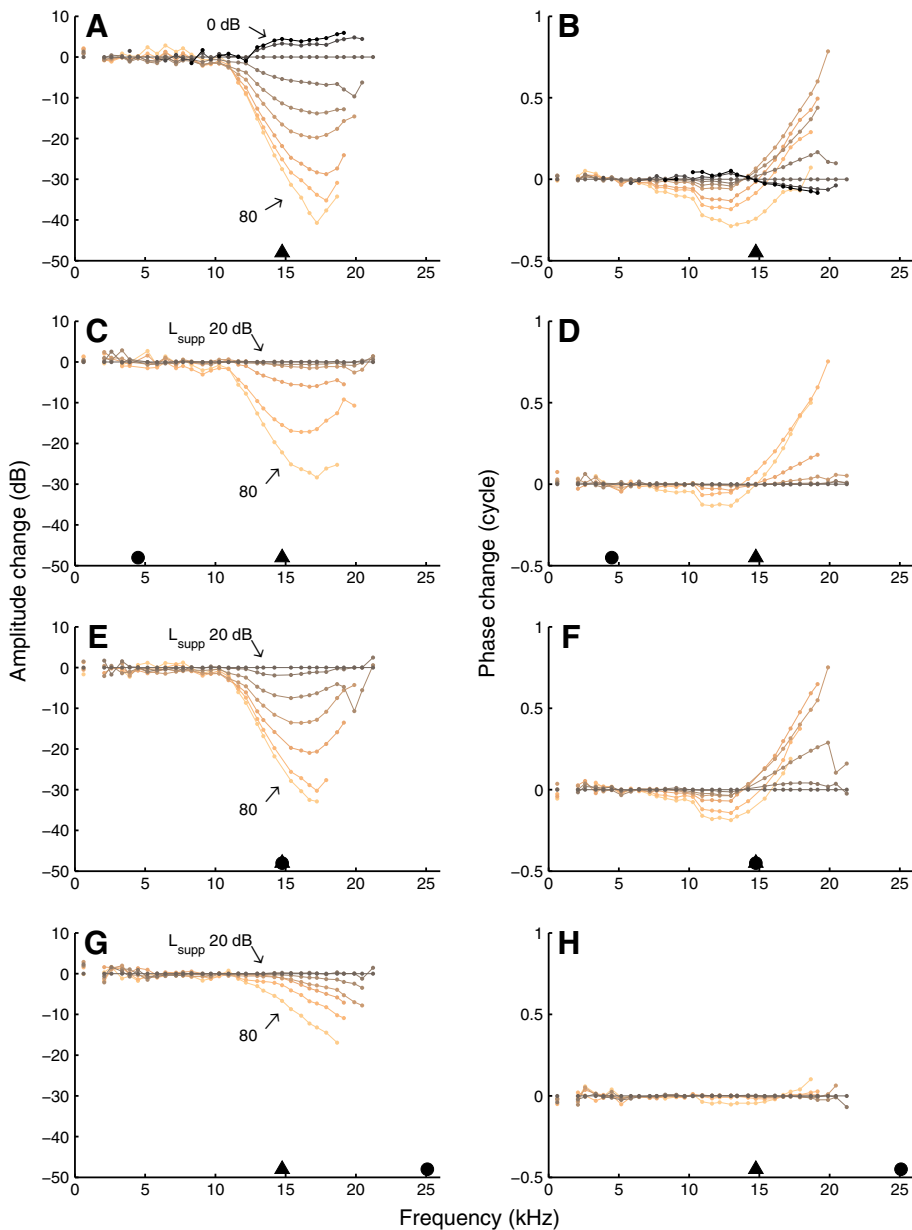


FIG. 2. Amplitude change (*left panels*) and phase change (*right panels*) induced by increasing overall intensity (**A, B**) or the intensity of a suppressor below CF (**C, D**), near CF (**E, F**), or above CF (**G, H**). The curves were obtained by referencing the data of Figure 1 to the response to the 20-dB-SPL equal intensity data, thus emphasizing deviation from (near) linearity. Layout and symbols as in Figure 1. Suppressor components are not shown in **C–H**.

focuses on the nonlinear aspects of the BM recordings (Versteegh and Van der Heijden 2012)—a linear cochlea would produce horizontal lines in each of the panels. The use of a low-intensity reference facilitates the comparison between compression and suppression (Cooper 1996).

The 0- and 10-dB-SPL curves in Figure 2A show positive values near CF, reflecting a larger sensitivity than the 20-dB-SPL baseline. The growth of the response was compressive from the lowest intensities tested (Fig. 1A), so the 20-dB-SPL reference condition is likely to reflect a certain degree of baseline suppression among its components. The use of a still lower-intensity reference condition would have reduced this baseline suppression, but would also have restricted the range of measurable probe responses to a narrow band around CF. Our choice of a 20-dB

reference was a compromise between minimizing baseline suppression and widening the range of probe frequencies. The price for the compromise is the underestimation of the “true” amplitude effects by 0–6 dB and of the phase effects by 0–0.1 cycle, depending on probe frequency.

The families of amplitude and phase curves obtained with equal-amplitude stimuli (Fig. 2A, B), a below-CF suppressor (Fig. 2C, D), and a near-CF suppressor (Fig. 2E, F) were very similar. Thus, these three ways of changing the stimulus intensity had virtually the same nonlinear effects over a wide range of probe frequencies. For these three datasets, the largest nonlinear amplitude changes were found for probes just above CF. The corresponding phase changes were systematic but complex. Phase pivoted around a frequency near CF as intensity increased

from 0 to 50 dB SPL (Fig. 2B). Below the pivoting frequency, phase acquired a lag; above the pivoting frequency, a lead. This pivoting pattern resembles phase effects in single-tone responses of the AN (Anderson et al. 1971; Palmer and Shackleton 2009) and the BM (Robles and Ruggero 2001), but the size of the phase effects reported here is larger than that of single-tone responses, especially above CF (Versteegh and Van der Heijden 2012). At the highest intensities, pivoting gave way to phase lags occurring over a wider frequency range. Again (as in Fig. 1), the differences in spacing of the families of curves reflect variations in threshold and rate of growth of suppression, but when matching the “effective level” of the suppressors, these differences largely disappear.

We estimated $f_{\min, \text{Amp}}$, the lowest probe frequency for which systematic amplitude shifts occurred, by plotting the variance across the curves of Figure 1A against probe frequency and assessing where the variance became elevated above the low-frequency baseline variance. This yielded $f_{\min, \text{Amp}} = 11.0 \text{ kHz} = 0.74 \times \text{CF}$. For all five cochleae tested, we obtained $f_{\min, \text{Amp}} = (0.71 \pm 0.04) \times \text{CF}$ ($N=5$). This is comparable to the range reported by Rhode (Figs. 2 and 3 of 2007b). Applying the same procedure to the phase data, the estimated lowest probe frequency showing systematic phase effects was $f_{\min, \text{Phase}} = 7.2 \text{ kHz} = 0.49 \times \text{CF}$ for the data of Figure 2B, and $f_{\min, \text{Phase}} = (0.54 \pm 0.09) \times \text{CF}$ ($N=5$) overall, comparable to the phase data reported by Rhode (Fig. 12 of 2007b).

The data obtained with the above-CF suppressor (Fig. 2G, H) differed from the other three datasets in several respects. Its amplitude changes were shifted toward higher-probe frequencies; amplitude changes did not peak at a frequency just above CF; and phase changes only occurred at the highest suppressor intensity (80 dB SPL). The deviating character of above-CF suppressors is elaborated in the next section.

An alternative view on the amplitude and phase changes was obtained by casting the data of Figure 2 in a contour plot (Fig. 3). This method more clearly illustrates that increasing the suppressor frequency beyond CF caused the frequency region of most affected probes to shift upward (Fig. 3G, H). This upward shift was found in all five cochleae tested. The contour plots also clarify the complex pattern of phase shifts (Fig. 3, right column), which was similar in the other cochleae. The phase shifts varied nonmonotonically with both probe frequency and suppressor intensity. The phase contours also clearly illustrate that the customary choice of near-CF probes amounts to selecting a subset of stimulus conditions (indicated in Fig. 3 by the *vertical dashed lines*) that is dominated by transitions between lags and leads. Slight inaccuracies in the CF estimates will therefore easily lead to reversals in the observed phase shifts, and this likely explains the discrepancies in the literature on suppressor-induced phase shifts

(Nuttall and Dolan 1993; Rhode and Cooper 1993), as previously suggested by Robles and Ruggero (2001).

Different frequency tuning of high-side and low-side suppression

In Figures 1, 2, and 3, three representative suppressor frequencies were selected to illustrate the major effects of varying suppressor frequency. A more complete analysis of the role of suppressor frequency, using data obtained with the entire set of suppressor frequencies, is shown in Figures 4 and 5. For two suppressor intensities, the amplitude and phase changes are shown as a function of both probe frequency and suppressor frequency. This display facilitates the evaluation of the frequency tuning of suppression. Note that the diagonals in Figures 4 and 5 demarcate low-side suppression ($f_{\text{supp}} < f_{\text{low}}$; below the diagonal) and high-side suppression.

For 50-dB-SPL suppressors (upper panels of Figs. 4 and 5), suppression was restricted to probes and suppressors around CF. Suppressors just below CF caused the largest amplitude and phase changes. For these suppressors, the amplitude changes peaked for probe frequencies just above CF, whereas the phase shifts kept growing with probe frequency (compare Fig. 2). The diagonal orientation of the contour lines for suppressor frequencies above CF, which is visible in both the amplitude and the phase data, shows that increasing the suppressor frequency beyond CF caused the frequency region of affected probes to shift upward, too.

The frequency selectivity of 80-dB-SPL suppressors (lower panels of Figs. 4 and 5) differed from that of the 50-dB-SPL suppressors in two respects. First, the range of effective suppressors was extended downward to arbitrarily low-suppressor frequencies. Second, the range of probes that underwent phase shifts was extended toward lower probe frequencies (down to ~ 1 octave below CF), and these below-CF probes always acquired phase lags. The 80-dB-SPL data revealed a clear contrast between low-side suppression ($f_{\text{supp}} < f_{\text{probe}}$) and high-side suppression. In both amplitude data (lower left panels) and phase data (lower right panels), the contour lines tended to have a vertical orientation below the diagonal $f_{\text{supp}} = f_{\text{probe}}$. This means that all of the low-side 80-dB-SPL suppressors had the same effects on the probe responses, independent of suppressor frequency (as long as it did not exceed probe frequency). This observation generalizes previous observations on near-CF probes (Cooper 1996; Rhode and Recio 2001b; Rhode 2007b). For the high-side suppressors, the orientation of the contour lines turned diagonal, signaling the same upward frequency shift of affected probes that was observed for the above-CF suppressors at 50 dB SPL. Thus, the similar frequency tuning of low-side and high-side suppression reported for near-CF

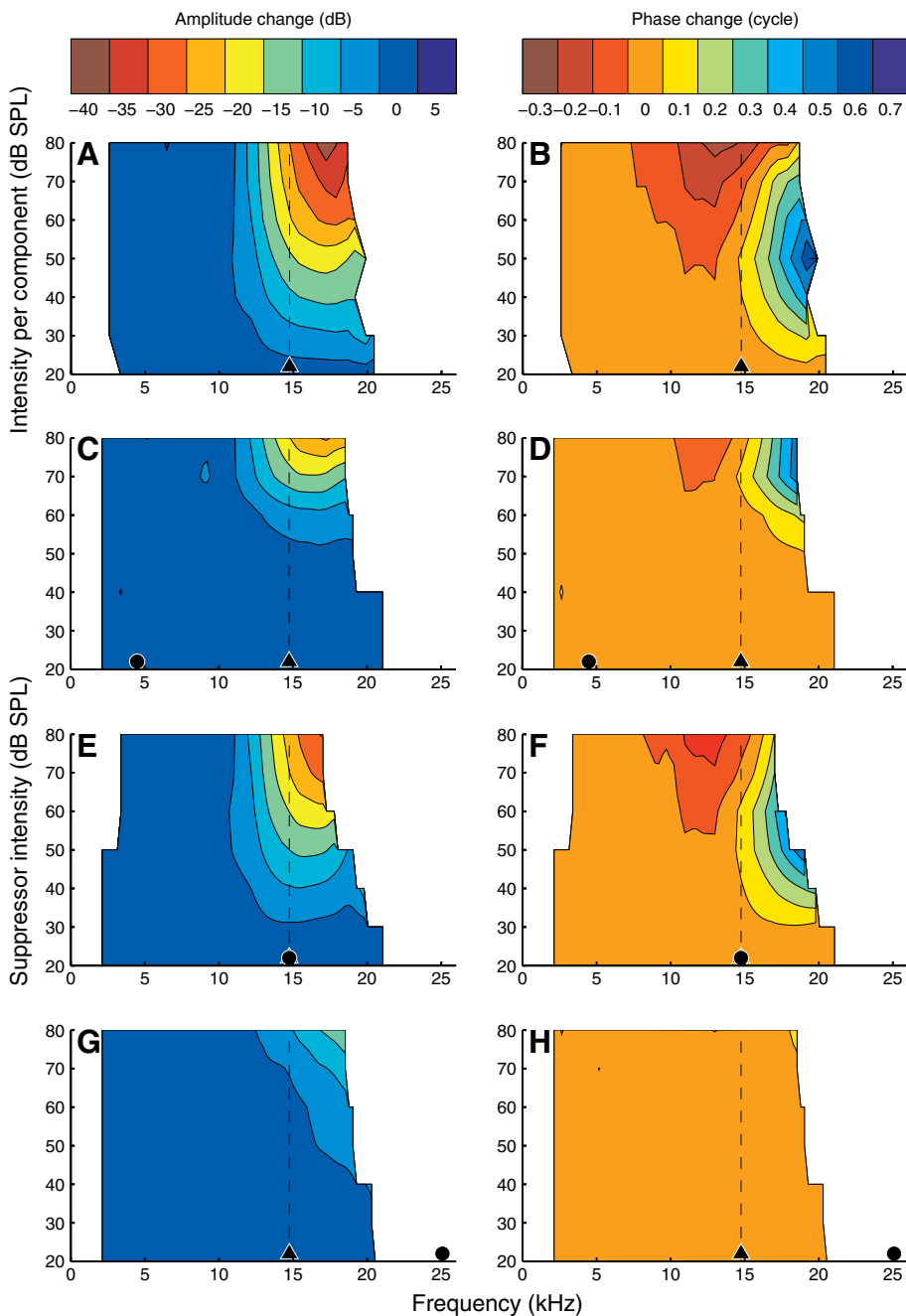


FIG. 3. Contour plots of amplitude and phase change. The data of Figure 2 are displayed as filled contour plots. *Color bars* above **A** and **B** quantify the changes in amplitude (*left panels*) and phase (*right panels*). Layout and symbols as in Figures 1 and 2. *Vertical dashed lines* mark the data for CF probes.

probes (Fig. 10 of Ruggero et al. (1992)) no longer holds when exploring a wider range of probe frequencies.

The near-diagonal orientation of the amplitude and phase contours above the main diagonal (all panels of Figs. 4 and 5) reveals that the amount of high-side suppression (and associated phase shifts) is strongly determined by the *frequency spacing between probe and suppressor*. An interpretation of this observation in terms of the limited spatial scope of high-side suppressors is presented in the Discussion.

The amount of suppression and the size of the phase shifts varied across animals, as is apparent from a detailed comparison between Figures 4 and 5. For instance, in Figure 5, both the maximum amount of

suppression for above-CF probes and the phase shifts for below-CF probes were larger than in Figure 4. The systematic effects discussed above, however, were consistently found in all five cochleae of this study.

The phase data (right panels of Figs. 4 and 5) provide further insight into the complex but systematic effects that suppressors have on the response phase of probes and extends the findings of other studies (Rhode and Cooper 1993; Cooper 1996; Rhode and Recio 2001a, b; Rhode 2007b). In addition to the nonmonotonic variation of probe phase with probe frequency and suppressor intensity (Figs. 2 and 3), the phase shifts also varied nonmonotonically with suppressor frequency. As discussed in connection with

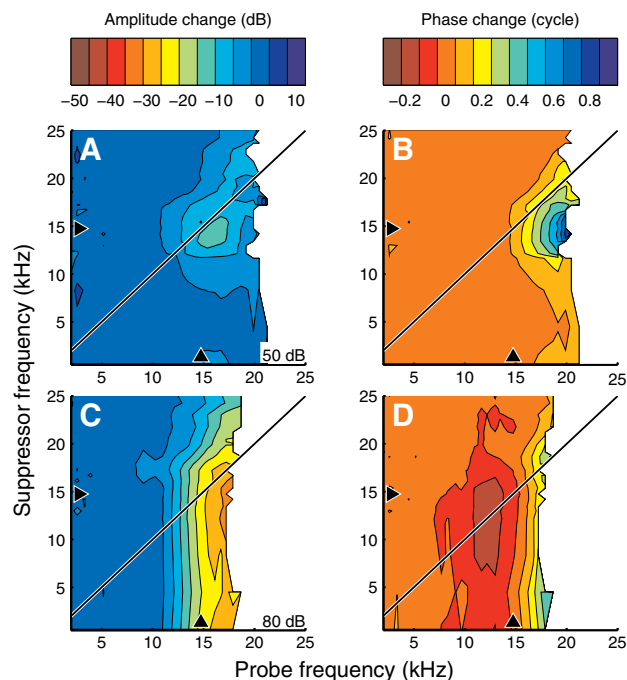


FIG. 4. Dependence of suppression on probe frequency and suppressor frequency. Amplitude changes (left panels) and phase changes (right panels) induced by 50-dB-SPL suppressors (upper panels) and 80-dB-SPL suppressors (lower panels) are shown as filled contour plots. Black triangles indicate CF (14.8 kHz). Color bars quantify the changes. Experiment RG12420.

Figure 3, the direction of the phase shifts depends critically on probe frequency, and this is also relevant

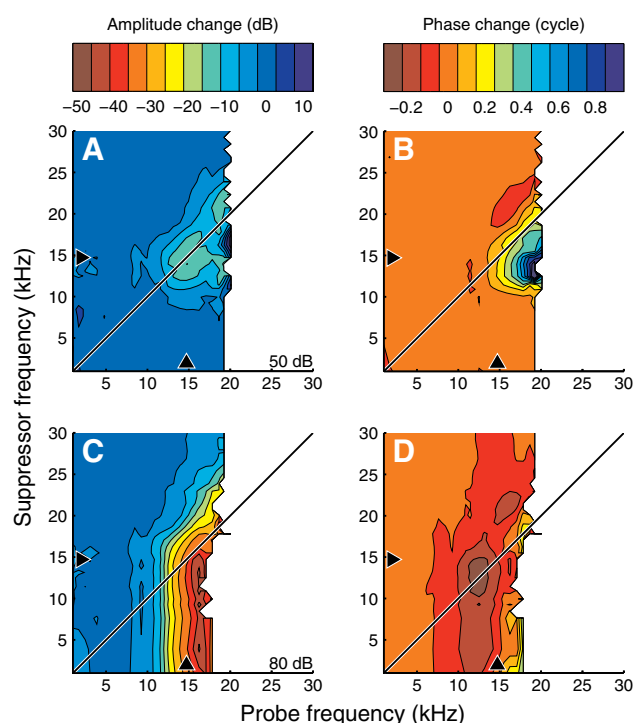


FIG. 5. As Figure 4, but for a different cochlea. CF was 14.7 kHz. Experiment RG12449.

when evaluating the role of suppressor frequency f_{supp} . For instance, when varying f_{supp} (vertical sections of Figs. 4 and 5), the phase shift imposed by an 80-dB-SPL suppressor on a below-CF probe will vary nonmonotonically, showing a peak *lag* for f_{supp} just below CF. On the other hand, the combination of a 50-dB-SPL suppressor and an above-CF probe will also produce a nonmonotonic variation with f_{supp} , but this time it has a peak *lead* for f_{supp} around CF. As noted above, and for the same reasons, the common choice of near-CF probes easily leads to discrepancies across data sets.

Large phase shifts in above-CF probes

Near-CF probes, the most common choice of probe in two-tone suppression studies, often showed small phase shifts compared to non-CF probes (Fig. 2). Rhode (2007b) studied the effects of CF suppressors on non-CF probes, and reported phase shifts up to 0.5 cycle. Our data do not have the restriction that either f_{probe} or f_{supp} equals CF, allowing us to explore phase shifts for many more $(f_{\text{probe}}, f_{\text{supp}})$ combinations. Figure 6 shows a few of the largest phase changes encountered. In one case (*closed symbols*), the phase shifts were induced by collectively changing the intensities of all components; in all other cases (*open symbols*), the phase shifts were induced by varying the intensity of a single suppressor component. Phase leads grew with probe frequency and exceeded one cycle in some cases (Fig. 6A). In Figure 6B, the phase shifts for the $(f_{\text{probe}}, f_{\text{supp}})$ combinations that led to maximal phase shifts in Figure 6A are plotted as a function of suppressor intensity. (Note that the fine frequency spacing in Figure 6A prevents any unwrapping errors in Figure 6B.) The growth of the phase leads was steep; it typically occurred over a narrow range (<30 dB) of suppressor intensities. The most extreme example of this steep growth (Fig. 6, *red squares*) was a phase lead of ~ 1.2 cycle occurring within a 20-dB increase of suppressor intensity!

Growth of suppressive effects with suppressor intensity

Figure 7 illustrates how the amount of suppression, or amplitude change, and the associated phase change varied with suppressor intensity L_{supp} . Many aspects of the growth of suppression with L_{supp} confirm and generalize previous observations from two-tone suppression (Nuttall and Dolan 1993; Cooper 1996; Cooper and Rhode 1996; Rhode 2007b). For any probe frequency, below-CF suppressors required a fairly high L_{supp} (>50 dB SPL) to start suppressing the probes. This threshold of suppression did not vary much with probe frequency, but the rate of suppression (ROS; the

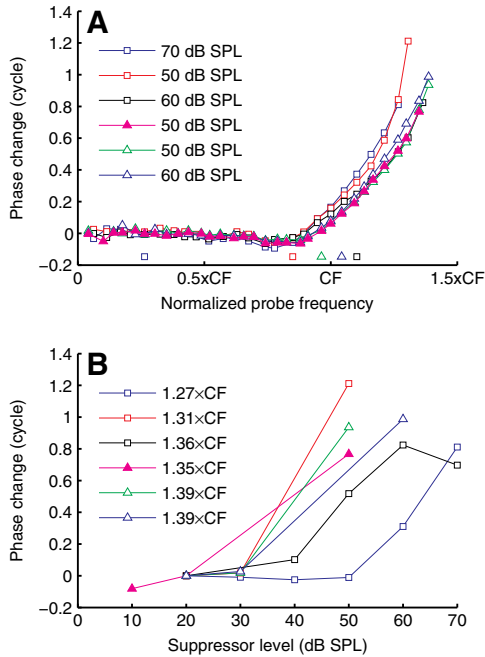


FIG. 6. Examples of large phase shifts from two cochleae (RG12420, CF=14.7 kHz, *triangles*; RG12449, CF=14.8 kHz, *squares*). **A** Phase changes induced by single-tone suppressors (*open symbols*) and wideband intensity increments (*solid symbols*), compared to their 20-dB reference, and plotted against normalized probe frequency. Suppressor intensity is indicated in the graph. Normalized suppressor frequency is indicated by the solitary symbols close to the abscissa. **B** The phase change of the probes associated with the peak values of **A** as a function of suppressor intensity. Symbols of **A** and **B** are matching; probe frequency is indicated in the graph. Peak values in **A** and **B** are identical.

downward slope of the curves) increased markedly with increasing probe frequency, exceeding 1 dB/dB for probes near CF and above CF (Fig. 7A).

Near-CF suppressors (Fig. 7C) had a lower threshold of suppression (~ 20 dB SPL), but the ROS was systematically shallower than for the low-side suppressors of Figure 7A. Again, the threshold of suppression did not depend markedly on probe frequency, whereas the ROS increased systematically with probe frequency. (The dependence of ROS on probe and suppressor frequencies will be elaborated on below.)

The variation of phase shifts with L_{supp} was nonmonotonic for below-CF suppressors (Fig. 7B) and near-CF suppressors (Fig. 7D). With increasing L_{supp} , a phase lead developed, peaked, and shrunk, often turning into a lag at the highest suppressor intensities. The size of the peak lead increased with increasing probe frequency. The common choice of CF probes (*thick lines*) led to relatively small phase effects when compared to above-CF probes.

The above-CF suppressor (Fig. 7E) had a threshold of suppression of ~ 30 dB SPL, and its initial ROS was shallower than that of the below-CF and near-CF suppressors. Only at the highest suppressor intensities

(>80 dB SPL) did the ROS become steeper. The phase shifts induced by the above-CF suppressor (Fig. 7F) deviated from the phase shifts induced by below-CF and near-CF suppressors (Fig. 7B, D) in that phase lags were not preceded by phase leads at lower suppressor intensities. The highest (90-dB-SPL) intensity of the above-CF suppressor produced a phase lead for the highest (>17 kHz) above-CF probes (Fig. 7F). This high-intensity effect was observed only in the cochlea shown here, possibly because it was the only experiment in which we used suppressor intensities above 80 dB SPL.

The similarities between the upper two rows of Figure 7 and their similarity to data obtained with wideband intensity increments (Fig. 6 of Versteegh and Van der Heijden (2012)) suggest that the following three ways of increasing stimulus intensity:

- a wideband intensity increment
- adding a below-CF suppressor
- adding a near-CF suppressor

had virtually the same effects after proper matching of their effective intensities. In contrast, the effects of adding an above-CF suppressor (bottom row of Figure 7) appeared to be qualitatively different. The similarities and contrasts are clearly illustrated when plotting the phase change $\Delta\Phi$ directly against the amplitude change ΔA (*cf.* Fig. 5 of Cooper 1996). This eliminates the intensity from the display and focuses on the collective changes observed in the probes (Figs. 6 and 7 of Versteegh and Van der Heijden 2012). Each panel of Figure 8 shows a family of $\Delta\Phi$ - ΔA curves obtained with a given suppressor, with each individual curve corresponding to a probe frequency. The curves start in the origin and move away as intensity is increased. Increasing the intensity of all tones together (Fig. 8A), of a below-CF suppressor (Fig. 8B), and of a near-CF suppressor (Fig. 8C) all yielded highly similar patterns of counter-clockwise rotation with increasing f_{probe} . The above-CF suppressor (Fig. 8D) had a qualitatively different effect on the probe responses, as illustrated by the different shape of the family of curves. This qualitative difference confirms the deviating character of high-side suppression.

The systematic patterns of Figure 8A-C include small *positive* amplitude changes for probes at frequencies $\sim \text{CF}/2$, seen as a leftward excursion of the curves (*dark blue lines*). Remarkably, the amplitude of these probe responses *increased* upon the introduction of the suppressor. This low-frequency “anti-suppression” is visible in Figure 4 of Rhode (2007b), although it was not discussed by the author. Antisuppression is closely related to the nonlinear expansive growth of below-CF responses found by Cooper (2000a), Rhode (2007a), and Versteegh and Van der Heijden (2012). Unlike the more familiar compressive behavior, it shows an *increase* of sensitivity for higher stimulus intensities.

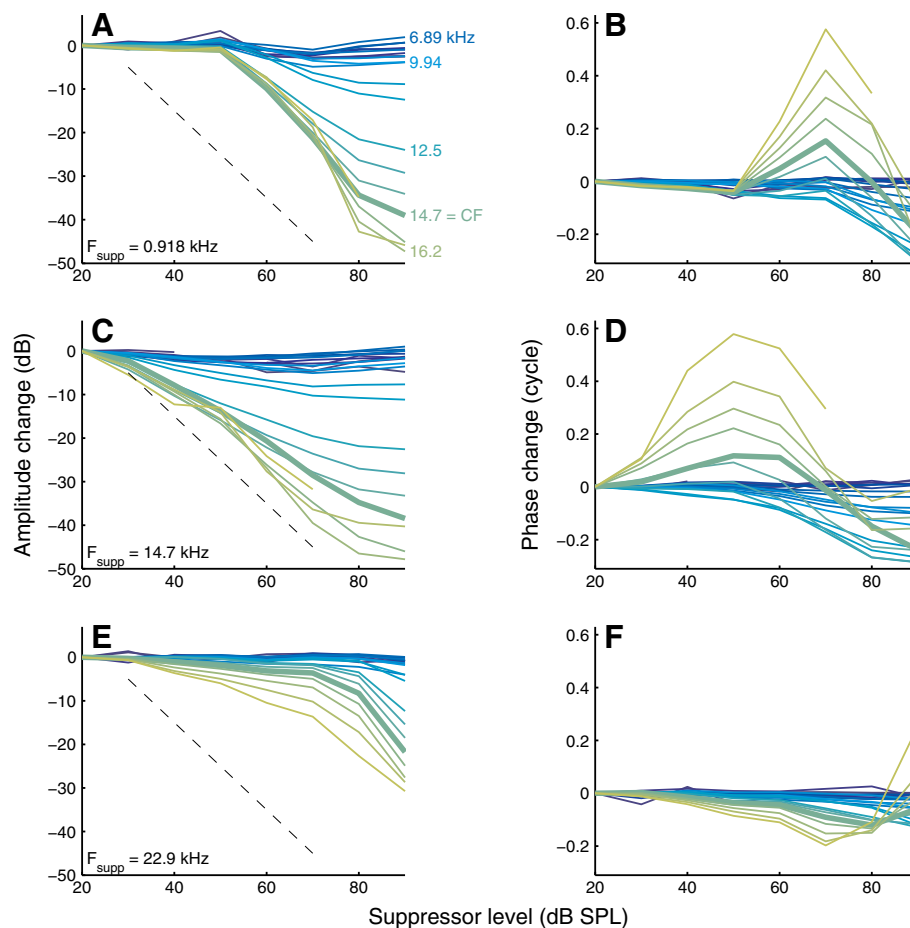


FIG. 7. Dependence of amplitude and phase of probe responses on suppressor intensity. For a below-CF (**A, B**), near-CF (**C, D**), and above-CF (**E, F**) suppressor the amplitude (*left panels*) and phase (*right panels*) of the entire collection of probes is shown. Suppressor frequency is indicated in the graphs. The gradual transition from blue to green curves corresponds to increasing probe frequencies, a subset of which is indicated in **A**. *Thick lines* are used for the curves of CF probes (14.7 kHz). The *dashed black lines* indicate a slope of -1 dB/dB. Experiment RG12449.

ROS was evaluated by determining the slope of the steepest portion of those amplitude curves of Figure 7 that contained a sufficient number of significant points to justify slope estimates (see “Materials and methods” section). The effect of suppressor frequency f_{supp} on ROS is shown for two cochleae in Figure 9A, B. For f_{supp} up to $\sim \text{CF}/2$, ROS was fairly independent of f_{supp} , and this was true for all probe frequencies. When increasing f_{supp} beyond $\text{CF}/2$, ROS steadily decreased, and this decrease continued up to suppressor frequencies well above CF. A similar dependence of ROS on suppressor frequency was found in all five cochleae, as illustrated in Figure 9C for CF probes. The dependence of ROS on f_{probe} was always simple: ROS decreased monotonically with decreasing f_{probe} .

The contour plot of Figure 6D displays ROS as a function of both f_{supp} and f_{probe} . The vertical alignment of contour lines well below CF illustrates that for sufficiently low f_{supp} , ROS was determined by f_{probe} alone and independent of f_{supp} . For near-CF and above-CF f_{supp} , however, the contours turned diagonal, indicating a constancy of ROS when varying f_{supp} and f_{probe} together in a fixed ratio. Stated differently, in this frequency region, the ROS was primarily determined by the frequency *spacing* between probe

and suppressor, rather than by probe frequency alone.

BM displacement as a predictor of suppression

Previous work has shown that the amount of suppression of near-CF probes is well predicted by the BM displacement evoked by low-side suppressors (Patuzzi et al. 1984; Geisler and Nuttall 1997), but not for high-side suppressors (Cooper 1996). Those studies also showed that adding a low-side suppressor to a probe always increased the *total* BM displacement, even though the Fourier component at the probe frequency was suppressed. On a closely related note, a low-side suppressor must dominate the overall BM displacement in order to produce sizeable suppression. In contrast, introducing a high-side suppressor often resulted in a decrease in overall BM displacement, and high-side suppressors could well suppress probes without dominating the displacement response (Cooper 1996; Cooper and Rhode 1996; Rhode and Recio 2001b; Rhode 2007b). The independent variation of probe and suppression frequencies allowed us to examine this contrast more comprehensively than previous studies.

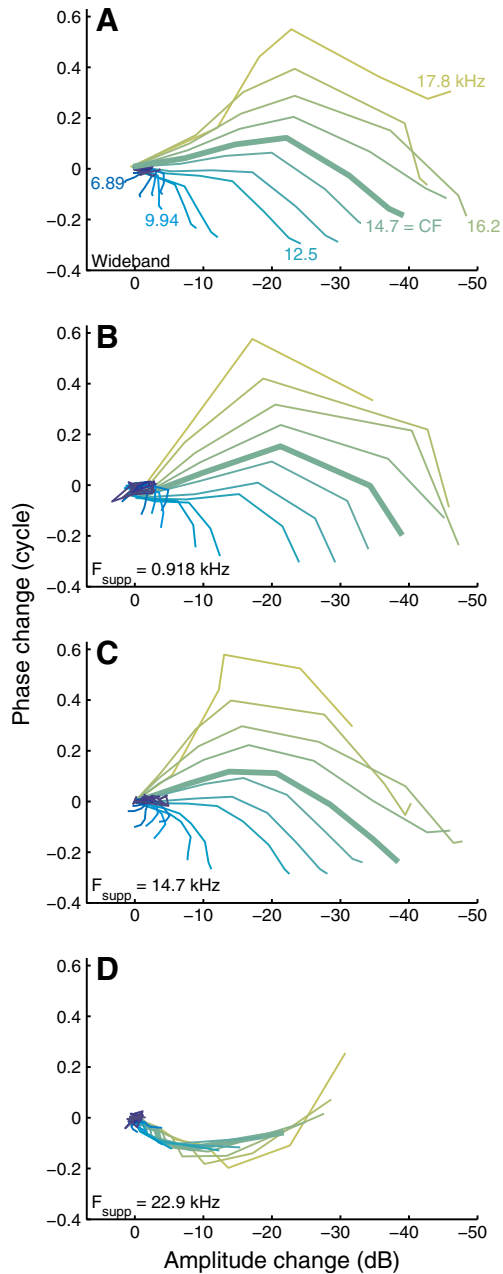


FIG. 8. Phase change against amplitude change for different suppressors. Wideband intensity increments (**A**); below-CF (**B**), near-CF (**C**), and above-CF (**D**) suppressor as indicated in the graphs. Different colors correspond to different probe frequencies and a subset is indicated in **A**. The $f_{\text{probe}} = \text{CF}$ (14.7 kHz) line is thicker than the others. Same data as shown in Figure 7.

Figure 10A–F show the amplitude (*left column*) and phase (*right column*) of probe responses as a function of the displacement amplitude of the suppressor component. Each panel shows the amplitude or phase of a single probe component. The first, second, and third row show a below-CF, near-CF, and above-CF probe, respectively. The different curves within each panel correspond to the different suppressor frequencies. Within each panel, all the curves corresponding to

below-CF and near-CF suppressors virtually overlapped, confirming that BM displacement was a reliable predictor of both the amount of suppression (i.e., amplitude change) and phase change for these suppressor frequencies. The minimum BM displacement for these suppressors to be effective did not vary much with probe frequency; for all five cochleae it amounted to 1–3 nm, in agreement with the 1–5 nm for CF probes reported by Cooper (1996). For above-CF suppressor frequencies, however, the curves shifted to the left, indicating that the same changes in probe amplitude and phase occurred for progressively smaller BM displacements when the suppressor frequency was increased beyond CF.

The dashed lines in Figure 10A, C, and E are isodisplacement contours, marking those combinations of probe amplitude and suppressor amplitude for which their (Pythagorean) sum equals the amplitude of the unsuppressed probe (*cf.* Fig. 2 of Cooper (1996)). In a genuine two-tone paradigm, the dashed curve would separate data points for which the suppressor caused an overall *decrease* of mean-square BM displacement (left to the dashed curve) from points corresponding to an overall *increase* of BM displacement. Although this demarcation ignores the contribution of the other probes of our wideband stimulus, its relation to the data is very similar to that reported by Cooper (1996) for genuine two-tone data. This suggests a similar interpretation, namely that all below-CF and near-CF suppressors caused an increase in overall BM displacement, and that only above-CF suppressors ever caused a decrease of BM displacement. A direct analysis of overall BM displacement, which incorporates the contributions from all stimulus components (Fig. 10G), confirmed this interpretation. For most suppressor frequencies, in order for suppression to occur, the suppressor must dominate BM displacement, hence the increase of overall BM displacement with suppressor intensity. Only for the highest suppressor frequencies did the overall BM displacement decrease with increasing L_{supp} . The most extreme cases are those in which the suppressor (e.g., $f_{\text{supp}} = 29.2$ kHz in Fig. 10G), did not by itself cause a significant BM displacement (hence its absence from Fig. 10A–F), but still suppressed the overall BM displacement produced by the other stimulus components. Such “phantom suppressors” are likely to exert their suppressive effects at a location basal to the recording site, nearer to their own peak region.

The below-CF probe (Fig. 10A) differed from the near-CF and above-CF probes (Fig. 10C, E) in one important aspect. Unlike the latter two, the below-CF probe was only suppressed by “dominant suppressors”, i.e., suppressors exceeding the probe in BM displacement. (Note that all the curves in Figure 10A lie to the right of the dashed line.) Apparently, it requires a combination of a near-CF (or above-CF) probe and a high-side suppressor for a non-dominant suppressor to

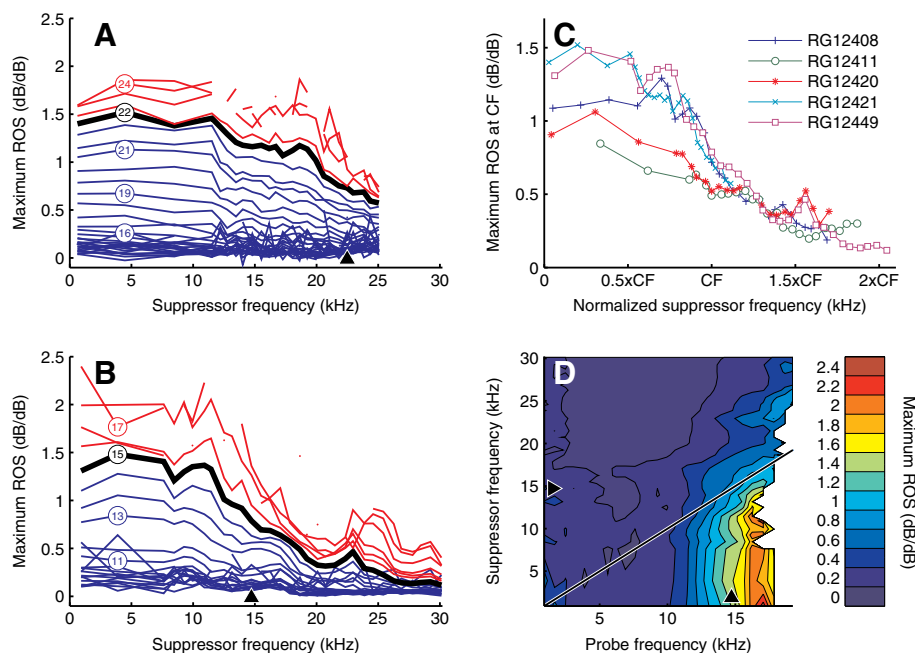


FIG. 9. Maximum rate of suppression (ROS) derived from the reduction of probe response amplitude with suppressor intensity (see text). **A, B** ROS versus suppressor frequency. Different curves represent different probe frequencies, a subset of which is indicated in kHz by the numbers enclosed by circles. Below-CF probes are shown in blue, CF probes are shown in black and marked by thicker lines, and above-CF probes are shown in red. **C** ROS of CF probes for five cochleae, plotted against normalized suppressor frequency. **D** Contour plot showing ROS as a function of both probe frequency and suppressor frequency. Suppressor intensity was 80 dB SPL. ROS is quantified by the color bar to the right of the graph.

be effective. This claim is substantiated in Figure 10H, where the *gray area* marks the $(f_{\text{probe}}, f_{\text{supp}})$ combinations for which the probe was suppressed by at least 3 dB for any of the suppressor intensities (30–80 dB SPL). The black area marks the subset for which the suppressor was “non-dominant”, i.e., for which the suppressor displacement did not exceed the probe displacement. Regardless of probe frequency, nondominant suppressors were only effective for suppressor frequencies well above CF. This supports the hypothesis that nondominant suppressors actually exert their suppressive effects in a region basal to the recording site, where they still dominate the probe (see “Discussion” section).

Automatic gain control model

The similarity between the effects of wideband intensity increments and suppression by single tones (Figs. 2, 3, and 8) suggest that suppression may well be modeled by equal-amplitude responses. The challenge is to match the “effective levels” of the two types of suppression. There is no obvious relation between, say, an 80-dB-SPL, single-tone suppressor at 918 Hz and a collective increment of all 40 stimulus components to 65.5 dB SPL. Yet, these two stimulus conditions produce virtually the same amount of suppression for all probes (Fig. 11A). The success of BM displacement in predicting suppression and phase changes (Fig. 10), suggests the use of overall BM displacement as a means of equalizing the effective levels. In a previous publication, we presented an automatic gain control scheme that implemented this idea (Fig. 5 of Versteegh and Van der Heijden 2012), and this scheme can be readily applied to model the present data. In short, the flat-amplitude responses of Fig. 1 are used as the collection of transfer functions of a variable-

gain filter. The actual gain setting depends on the stimulus via negative feedback, and is determined by the RMS displacement at the *output* of the filter. Specifically, among all the possible gain settings of the filter that one is selected that produces the same output RMS when applied to the test stimulus as it produced for the flat-amplitude reference condition that yielded the gain setting. A detailed description can be found in Versteegh and Van der Heijden (2012). Importantly, the gain control model has no free parameters. The gain control scheme is a heuristic model of suppression rather than a physiologically realistic attempt to explain nonlinear interaction in the cochlea. Its most obvious flaw is the absence of spatial dimensions. Therefore, its performance is expected to be poor in situations in which the spatially distributed character of suppression is important (see “Discussion” section).

Figures 11A, B show that the gain control scheme produced accurate predictions for below-CF suppressors. For above-CF suppressors (Fig. 11C), the predictions tended to overestimate the amplitude (or underestimate the suppression) of near-CF probes. A comparison of predictions and data for the entire set of suppression frequencies is shown for two suppressor intensities: 50 dB SPL (Fig. 11D) and 80 dB SPL (Fig. 11E). Given the simplicity of the model (and the absence of free parameters for tweaking), the predictions are quite good. The most obvious flaw is the systematic overestimation of amplitude for above-CF suppressors, which is consistent with the failure of BM displacement to predict suppression by above-CF suppressors (Fig. 10). For the 50-dB-SPL suppressors (Fig. 11D), the response amplitude of above-CF probes was somewhat underestimated (i.e., suppression was overestimated) for suppressor frequencies just below CF. This secondary flaw might be caused by the

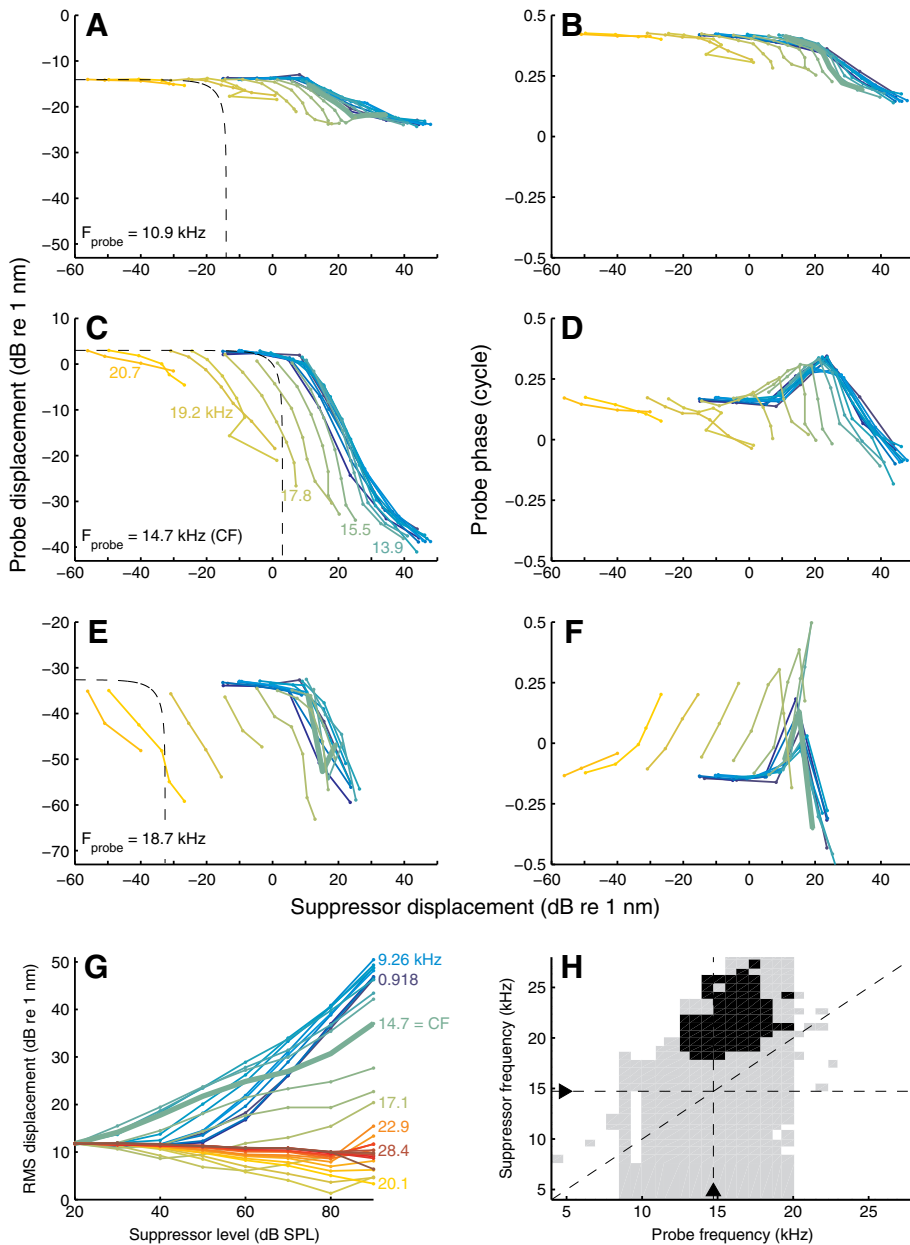


FIG. 10. The role of BM displacement magnitude of suppressors. Panels A–F show how the response amplitude (left) and phase (right) of a given probe vary with the magnitude of BM displacement evoked by suppressors. Different curves within each panel correspond to different suppressor frequencies. A selection of suppressor frequencies is indicated in C. With increasing suppressor frequency, line color gradually changes from blue to yellow. Different rows of panels correspond to different probe frequencies: a below-CF (A, B), near-CF (C, D), and above-CF (E, F) probe as indicated in the graphs. Black dashed curves indicate equality of probe-alone and probe+suppressor BM displacement (see text). In all panels, thick lines indicate CF (14.7 kHz) suppressors. G Total RMS displacement against suppressor intensity. Different lines represent different suppressor frequencies, a selection of which is indicated in the graph. Line color gradually changes from blue to red with increasing suppressor frequency. H Suppression by nondominant suppressors. The gray area marks the combinations of probe and suppressor frequencies for which at least 3 dB of suppression was found for any suppressor intensity. The black area is the subset of frequency pairings for which probe-induced BM displacement exceeded suppressor-induced displacement. Experiment RG12449.

larger role of high-side suppression in the flat-amplitude reference condition compared to the 50-dB-SPL suppressor just below CF. These flaws should not distract from the overall performance of the model. In the five cochleae tested, the gain control scheme accounted for 92.8 ± 3.2 and 92.6 ± 5.6 % of the variance in amplitude and phase, respectively.

DISCUSSION

Summary of main findings

(A) Below-CF suppressors, near-CF suppressors, and wideband intensity increments had very similar effects on probe responses, and this similarity

includes the complex phase effects (Figs. 1, 2, 3, 4, 5, and 8)

(B) The effects of above-CF suppressors were qualitatively different from the effects of below-CF and near-CF suppressors (Figs. 2, 3, 4, 5, 7, and 8)

(C) For below-CF and near-CF suppressors, suppressor frequency had no effect on the frequency range of most affected probes, but for above-CF suppressors, the frequency range of affected probes shifted upward with increasing suppressor frequency (Figs. 3, 4, and 5)

(D) Systematic suppression only occurred for probes having a frequency exceeding $(0.71 \pm 0.04) \times \text{CF}$ ($N=5$; Fig. 2)

(E) Lagging phase shifts occurred for probes at frequencies as low as $(0.54 \pm 0.09) \times \text{CF}$ ($N=5$; Fig. 2)

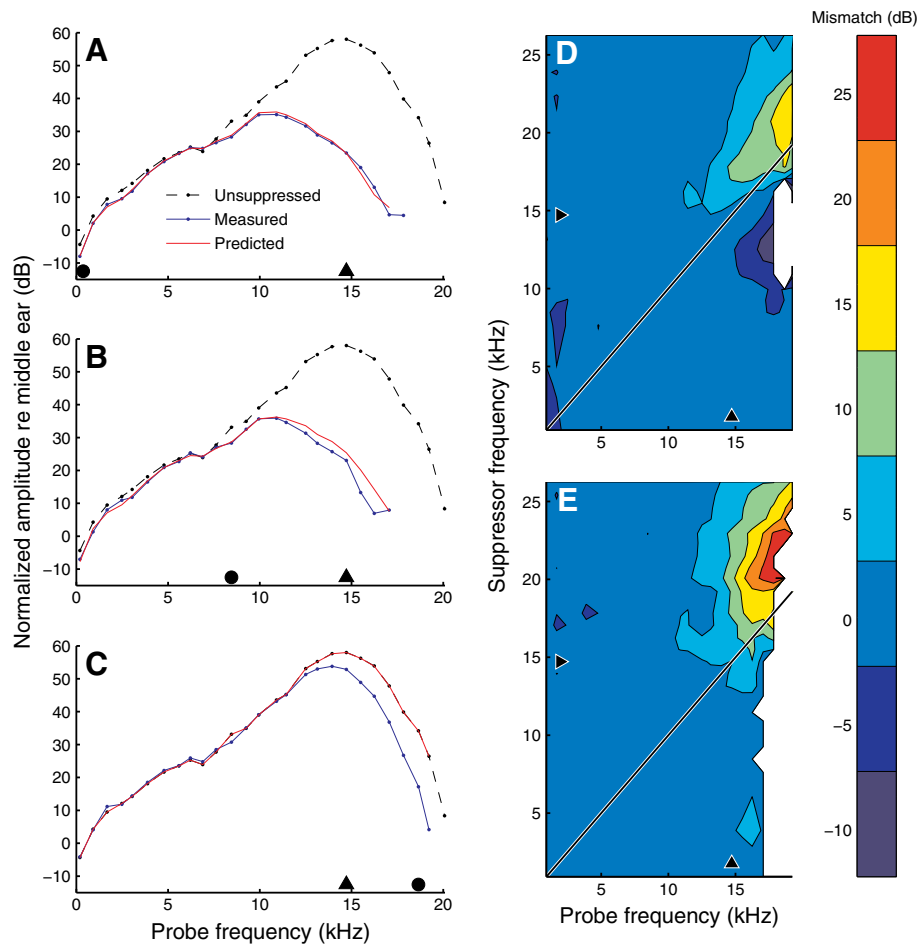


FIG. 11. Performance of a simple gain control model based on local BM displacement (see text). Measured and predicted BM response amplitudes for two below-CF suppressors (**A**, **B**), and an above-CF suppressor (**C**), each presented at 80 dB SPL. Suppressor frequency is indicated by *solid black circles* (918 Hz, 14.7 kHz, and 24.6 kHz, respectively). The *different lines* in each plot show: the unsuppressed (reference) response at 20 dB SPL (*black dashed line*); measured suppressed response (*blue solid line*); prediction of suppressed response from the model (*red solid line*). **D** and **E** show the model mismatch (predictions minus data) for all suppressor frequencies, with suppressor intensity equal to 50 and 80 dB SPL, respectively. *Black triangles* indicate CF (14.7 kHz). Experiment RG12449.

- (F) Responses to probes at $\sim 0.5 \times \text{CF}$ were often “anti-suppressed” by a few decibel by intense (80–90 dB-SPL) suppressors (Figs. 7 and 8)
- (G) Rate of suppression varied systematically with both suppressor frequency and probe frequency (Figs. 7 and 9)
- (H) Phase shifts varied nonmonotonically with suppressor intensity, suppressor frequency and probe frequency (Figs. 2, 3, 4, 5, 7, and 8)
- (I) Reversals of phase shifts (lag to lead or conversely) often occurred for probe frequencies close to CF (Figs. 2, 3, 4, 5, 7, and 8)
- (J) For above-CF probes, leading phase shifts exceeding one cycle were observed for near-CF suppressors at 50–60 dB SPL (Fig. 6)
- (K) BM displacement was a reliable predictor of suppression by below-CF and near-CF suppressors (Fig. 10)
- (L) For below-CF and near-CF suppressors, the minimum displacement for suppression (“threshold”) was quite independent of probe frequency (Fig. 10) and amounted to 1–3 nm
- (M) A simple gain control scheme based on BM displacement as a metric for “effective suppressor intensity” accurately predicted suppression and

- phase shifts by below-CF and near-CF suppressors from flat-amplitude responses (Fig. 11)
- (N) Even when including data for above-CF suppressors, the gain control scheme explained >90 % of the variance
- (O) In order to suppress any probe, below-CF suppressors and near-CF suppressors must dominate BM displacement (Fig. 10)
- (P) Suppression by nondominant suppressors only occurred for a restricted range of suppressors well above CF suppressing near-CF probes (Fig. 10H)

Several of these findings confirm and generalize earlier work, as addressed in “Results” section. Other findings appear to be new (C, J) or went unnoticed before (F). To us, however, the main value of the data is their completeness in the frequency domain, with probe and suppressor frequencies being independently varied. This completeness allows the straightforward use of scaling arguments (frequency to place conversion). As shown below, from this analysis, a picture of interacting traveling waves emerges that is surprisingly simple in some aspects (spatial buildup of suppression) and complex in other (competing phase effects). Most

importantly, it unifies seemingly independent observations both within this study and from previous work.

Traveling waves and the spatial buildup of suppression

We interpret the data in the framework of traveling waves whose propagation properties depend on the magnitude of local BM displacement. Specifically, larger BM displacements cause local propagation to be less efficient, and this reduction of “local forward gain” is frequency dependent (as is the gain itself). Thus, any wave traveling at the location participates in two ways:

1. It contributes to the local BM displacement
2. Its propagation is affected by the magnitude of the local BM displacement

Our aim is to analyze the second, probe-like, behavior. This task is complicated by the cumulative character of the effects. When arriving at the recording location, the wave carries a “travel history”—it has been shaped by the propagation properties along its entire path. The challenge is to dissect the consecutive local contributions from the accumulated effects.

The simplest case is low-side suppression by a suppressor well below CF. The suppressor dominates BM displacement (Fig. 10; see also: Cooper 1996; Geisler and Nuttall 1997) and the variations in displacement magnitude along the basal tail of the low-frequency suppressor are relatively minor (e.g., Figure 4A of Ren (2002)). Thus in the relevant region of the cochlea (the recording site and everything basal to it), the effects of the suppressor resemble those of a wideband gain control. This simplifies the analysis, because it renders suppressor frequency relatively unimportant, suggesting that it may be ignored when converting frequency to place. To fairly good approximation, then, the amplitude curves of Figure 1A, C can be viewed as spatial profiles of displacement magnitude along the BM. The main features are illustrated in the schematic diagram (Fig. 12).

By itself, a low-intensity probe evokes a traveling wave (Fig. 12A) consisting of a long basal tail followed by a narrow peak. Next, a high-intensity, low-frequency suppressor is added to the probe (Fig. 12B). The suppressor dominates the BM displacement over the entire range shown, but only affects the peak portion of the probe wave marked “suppressible” in Figure 12A and “suppressed” in Figure 12B.

The key feature shown in Figure 12B is the *spatial buildup of suppression*. The suppressor does not simply scale down the entire probe wave, but affects it in a gradual way, as reflected by the growing distance between the unsuppressed and suppressed profiles in

the travel direction. The onset of the divergence is indicated by the *black arrow* in Figure 12B. The spatial buildup of suppression corresponds (via scaling) to the divergence, below CF, of the amplitude curves in Figure 1A, C and to the negative slopes of the change-of-amplitude curves of Figure 2A, C. Suppression keeps accumulating beyond the peak of the unsuppressed probe profile, causing the peak of the suppressed probe wave to shift toward the base. Somewhat apical to the peak, suppression stops accumulating (*cf.* the settling of the curves of Fig. 2A, C beyond CF). In this apical portion beyond the peak, the suppressor no longer exerts a local effect on the probe wave, but the accumulated effect of suppression from the more basal region is not undone, either. As a result, the apical flanks of the unsuppressed and suppressed profiles do not further diverge, but become approximately parallel (on a log displacement scale).

The spatial buildup of suppression along the direction of wave propagation explains the systematic increase of ROS with probe frequency (Fig. 9; see also Fig. 4B, D of Rhode (2007b)). This is illustrated schematically in Fig. 13. Below-CF probes are recorded basal to their peak, where the probe wave has only just started to accumulate suppression (marked *b* in Fig. 13). For higher-frequency probes, the recording exposes a later stage of the wave (marked *a* in Fig. 13), where a wider spatial region has contributed to its suppression. When increasing the suppressor intensity, BM displacement grows over the entire range, increasing the amount of suppression (*blue curve* versus *red curve* in Fig. 13). The gradual buildup of suppression, however, causes the incremental amount of suppression (*double-headed arrows* in Fig. 13) to accumulate from base to apex. Thus, the growth of suppression is larger at the more apical location marked *a*. This explains, via scaling, why the growth of suppression with suppressor intensity is steeper (higher ROS values) for higher-frequency probes than for lower-frequency probes.

High-side suppression

High-side suppression is illustrated in Figure 12C. The frequency spacing between probe and suppressor is a key factor because it determines the region of overlapping excitation. If the spacing is too wide (*dashed red curve* in Fig. 12C), the suppressor is ineffective simply because it fails to dominate BM displacement in the suppressible portion of the probe wave. This explains the upward frequency shift of affected probes when suppressor frequency is increased above CF (Figs. 3, 4, and 5).

Several factors contribute to the shallow growth (low ROS values) of high-side suppression. First, it is

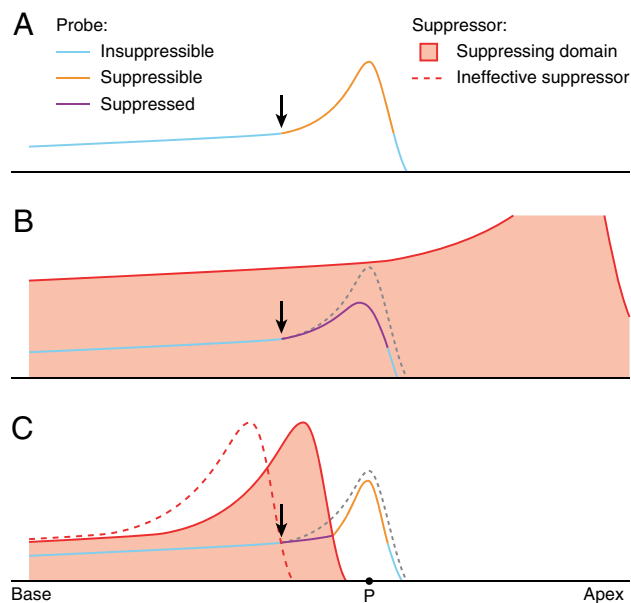


FIG. 12. Schematic spatial profiles of BM displacement magnitude. The vertical distance from the baseline indicates the amplitude of BM displacement in response to a stimulus component. A log scale of displacement is implied, meaning that parallel curves correspond to proportional variations in amplitude. **A** Displacement profile of unsuppressed probe wave. The peak portion is sensitive to suppressive effects. The basal tail and most apical portion are insensitive. The *black arrow* marks the transition between the insuppressible tail and the suppressible peak. **B** Adding a low-side suppressor does not affect the tail, but causes a progressive suppression of the probe wave, visible as a divergence between suppressed and unsuppressed probe profiles starting near the *black arrow* (see text). **C** High-side suppressors have limited overlap with the probe. Apical to the overlap region, the probe partially rebounds owing to its lowered amplitude (see text). At point P, suppression is observed but not the excitation of the suppressor (“phantom suppressor”). If the suppressor frequency is much higher than the probe frequency (*red dashed profile*), it will not affect the probe wave.

now the peak of the high-side suppressor wave that affects the probe wave (Fig. 12C), so *the compressive growth of the suppressor peak* contributes to the shallower growth of high-side suppression compared to low-side suppression (Fig. 9). The second factor is *the limited*

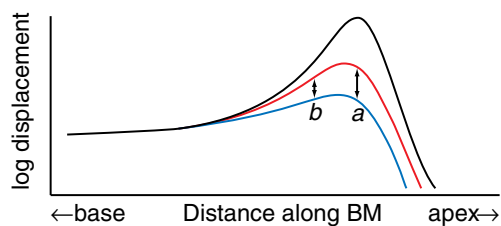


FIG. 13. Probe wave subjected to different amounts of suppression. *Black curve* unsuppressed probe wave. *Red curve* probe wave of reduced amplitude caused by a suppressor. *Blue curve* further reduction caused by increasing the suppressor intensity. The *arrows* mark the different growth of suppression at two locations labeled *a* and *b*.

spatial overlap of probe and suppressor waves. When increasing the frequency spacing between probe and suppressor, the spatial region contributing to suppressing the probe wave will shrink (Fig. 12C) and (as discussed above for low-side suppression) the ROS will become smaller. This explains the strong dependence of ROS on the frequency spacing between probes and high-side suppressors (cf. the diagonal contour lines in Figure 9D).

The third factor leading to low ROS values is the *rebound of the probe wave* once it has left the suppressor-dominated region (Fig. 12C). In the post-suppressor region it is the *probe* that dominates BM displacement, and the cochlear gain control causes the suppressed probe (which has a lower amplitude) to peak more steeply than the unsuppressed probe. In other words, the suppression of the probe by the suppressor is followed (and partially compensated) by a release from self-suppression. The latter two factors (limited spatial overlap and the rebound effect) may explain the observation of Cooper (1996) that “below-CF suppressor tones suppress the responses to CF probe tones at a greater rate than do above-CF suppressors, even when the different growth rates of the excitatory responses to the suppressor tones are taken into account.” Incidentally, the rebound effect represents a subtle exception from the general rule that the effects of suppression are equivalent to the effects of increasing stimulus intensity.

Both the variable overlap and the rebound effect are illustrated by an analysis of our high-side suppression data using frequency-place conversion. For reference, Figure 14A shows the spatial profile of suppression derived from the schematic diagram of Figure 12C. From base to apex, an initial unsuppressed portion is followed by a buildup of suppression (downward slope) and a partial rebound (upward slope). The final (most apical) part is flat, reflecting the absence of local contributions to suppression. The buildup of suppression is restricted to the spatial overlap region (Fig. 12C), which varies with the frequency spacing between suppressor and probe.

The crucial role of the frequency spacing between probe and suppressor necessitates some caution in the use of scaling. In order to use frequency as a proxy for longitudinal BM location, the two frequencies must be varied together in fixed proportion. We interpolated the data along the probe frequency axis (cf. the straight lines connecting the data points in Fig. 2) to exactly fix the frequency ratio across suppressor frequencies. Figure 14B shows the amount of suppression when varying f_{probe} and f_{supp} while keeping their ratio fixed. The $f_{\text{supp}}/f_{\text{probe}}$ ratios of the individual curves are indicated in the graph. By way of scaling, these curves should illustrate the spatial buildup of high-side suppression. Indeed, the curves in Figure 14B do show the

main features anticipated in Figure 14A. The accumulation of suppression is reflected by the common downward slope. The curves obtained with smaller $f_{\text{supp}}/f_{\text{probe}}$ ratios continue to accumulate suppression over a larger range, consistent with their larger spatial overlap. After parting from the common downward slope, each of the curves shows an upward turn, in agreement with the rebound after leaving the suppressor-dominated region (Fig. 12C). Four of the five cochleae showed both of these features (for the fifth one, RG12421, the range of tested probe frequencies was too narrow).

The bottom panel (Fig. 14C) shows the suppressor/probe ratio of BM displacement. Positive decibel values indicate a “dominant suppressor.” The correspondence to the upper panel (Fig. 14B) reveals that suppression stopped accumulating once the displace-

ment ratio dropped below ~ 30 dB. Thus, strong suppressor dominance was needed to locally suppress the probe. Further apical, the suppressor-evoked displacement dropped below that of the probe (“dominant probe”) and eventually became insignificant (“phantom suppressor”). The curves in Figure 14B show that the suppression measured at those more apical locations did not contain any local contributions, but was wholly inherited from the basal suppressor dominated region. This analysis further strengthens the evidence from Figure 10H that suppression observed with above-CF suppressors results from interactions occurring basal to the recording place (Kim et al. 1973; Geisler et al. 1990), and that the failure of local BM displacement to predict high-side suppression stems from the distributed character of suppression. Incidentally, low-side suppression is not really different in that respect. It is as spatially distributed as high-side suppression (or even more so; Fig. 12). The success of predicting low-side suppression from local BM displacement does *not* mean that low-side suppression is a local effect! The prediction just happens to work because BM displacement is fairly constant over the extended region contributing to suppression—which includes the recording location.

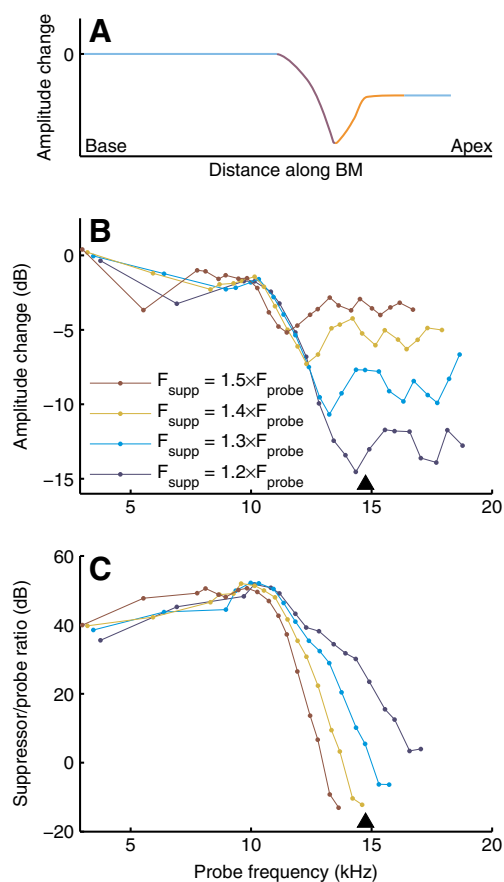


FIG. 14. The spatial buildup of high-side suppression. **A** Spatial profile of high-side suppression derived from the schematic wave envelopes of Figure 12C, using the same color coding. **B** The suppressor-induced amplitude change as a function of probe frequency, with probe and high-side suppressor varied in a fixed frequency ratio. Using a scaling argument (see text), these data illustrate the spatial buildup of high-side suppression, with low frequencies corresponding to the basal locations. **C** Suppressor/probe ratio of BM displacement corresponding to the data in panel B. Positive values indicate suppressor dominance. Experiment RG12449; 60-dB-SPL suppressor.

Quantifying the spatial growth of suppression

Given the gradual buildup of suppression along the propagation direction of the traveling wave, the natural metric of local suppression strength is the *amplitude loss per length unit*, i.e., the number of decibels lost per millimeter by a suppressed wave compared to a reference wave. Obviously, the best way to determine this metric is the direct comparison of BM vibration between adjacent longitudinal locations, but by applying a simple scaling procedure to the data of Figure 2A (and the analogous data from the other four cochleae) we obtained estimates for the loss gradient at a location ~ 300 μm basal to the best place of the wave, where local suppression peaks (see “Materials and methods” section). The result is shown in Figure 15. We used the 50-dB-SPL condition as the reference for which the loss gradient is 0 dB/mm by convention. Thus, positive loss gradient values mean that the suppressive loss per length unit was larger than for the 50-dB-SPL reference.

The use of a mid-intensity reference brings out the differences in sensitivity between the cochleae. Reduced sensitivity at low intensities is reflected by a shallower slope at small displacements. For instance, the left horizontal asymptote of the *green curve* (RG12411) in Figure 15 reveals that intensity decrements toward the lower end failed to further reduce the local losses—the response became almost linear at

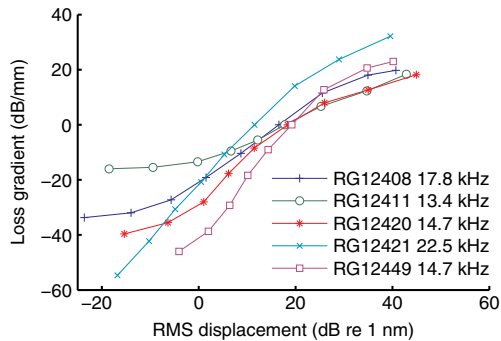


FIG. 15. Quantification of suppression strength by loss gradients. The loss gradient is the estimated amplitude loss per length unit of a suppressed wave relative to a reference wave (see text). The estimates were derived from responses to the wideband, equal-amplitude stimuli using the 50-dB-SPL data as a reference. Data from five cochleae are shown as indicated in the graph along with the CF of the recording sites.

the lowest intensities. The exact value of the asymptote is arbitrary, as it depends on the choice of reference. The slopes and ranges of the curves, however, are independent of the reference, and quantify how the spatial buildup of suppression depends on BM displacement.

For the two most sensitive cochleae (RG12449 and RG12421), the loss gradient increased by 75–85 dB/mm over the 80-dB range of stimulus intensities used. Thus, for each 125 μm traveled, the amplitude of the 80-dB-SPL wave lost ~ 10 dB compared to the more efficient propagation of the 0-dB-SPL wave. We also extracted estimates of loss gradients from the “local transfer functions” in Figures 2A and 3A of Ren et al. (2011), by dividing the largest intensity-induced amplitude differences by the distance between the two recording locations. This yielded a variation in loss gradient of 70–75 dB/mm over a 70-dB range of stimulus intensities, which is very similar to the estimates of Figure 15. Note that the consistency across experiments of the mid- and high-intensity data in Figure 15 (displacement >10 dB re 1 nm) is quite good, especially considering that variations in radial position of the beads easily cause amplitude differences >10 dB (Cooper 2000b).

Phase effects and their spatial buildup

Suppressor-induced phase shifts signify changes in the propagation speed (phase velocity) of the probe wave. Again, the challenge is to dissect consecutive local contributions from accumulated effects. For proper context, we briefly review the spatial profiles of phase and their relation to phase velocity as known from panoramic studies in single cochleae. The traveling wave has an initial high velocity, but when approaching its magnitude peak (best site), undergoes a sharp

transition to lower velocities. This spatial velocity profile is represented by the black line in Figure 16A; the transition point is marked T. Figure 16B shows the wave number or spatial frequency k , the number of cycles per length unit. Since k is inversely proportional to phase velocity, it jumps from lower to higher values. The wave phase $\Phi(x)$ at any point x along the BM is the integral of k :

$$\Phi(x) = \int_0^x k \, dx \quad (1)$$

This phase profile (Fig. 16C) shows the velocity transition near T as a sharp downward kink as reported in panoramic neural studies of single cochleae (Kim et al. 1980; Van der Heijden and Joris 2006). The kink is also visible in studies based on pooling data across different cochleae (Palmer and Shackleton 2009; Temchin et al. 2012), although the pooling is likely to have weakened the apparent sharpness in the latter studies.

How does suppression affect propagation speed? The phase effects observed with suppressors and wideband intensity increments (Figs. 2, 4, 5, and 7) signify a *softening of the transition from fast to slow propagation*. Basal to the transition point T, the probe wave is slowed down; apical to T, it is sped up (*brown lines* in Fig. 16). At T itself, wave velocity is unaffected—it “pivots” around T (Fig. 16A). Likewise, the transition of wave number (Fig. 16B) is softened and its profile also pivots around T. The local phase, being the integrated wave number, shows the softened velocity transition as a rounded downward bend that replaces the original sharp kink (Fig. 16C). Importantly, the point B at which the phase is unaffected by the suppressor lies apical to T, namely where the phase lag caused by the slower propagation prior to T has just been compensated by the phase lead accumulated by the faster propagation beyond T. This point B is close to the best site of the wave (*cf.* the constancy of phase near CF, Fig. 2). The phase shift relative to the unsuppressed phase profile is shown in Figure 16D. Its major features are consistent (via scaling) with the phase shift data in Figure 2B, D, E.

When the suppressor intensity is further increased (*ochre curve* in Fig. 16A), the portion of the probe wave basal to T continues to slow down, but the portion of the probe wave apical to T does not further speed up. In the accumulated phase (Fig. 16C), this produces a uniform shift in the lagging direction which replaces the pivoting around B. This phase shift corresponds (via scaling) to the widening of the probe–frequency range showing phase lags (highest suppressor intensities in Fig. 2B, D, F).

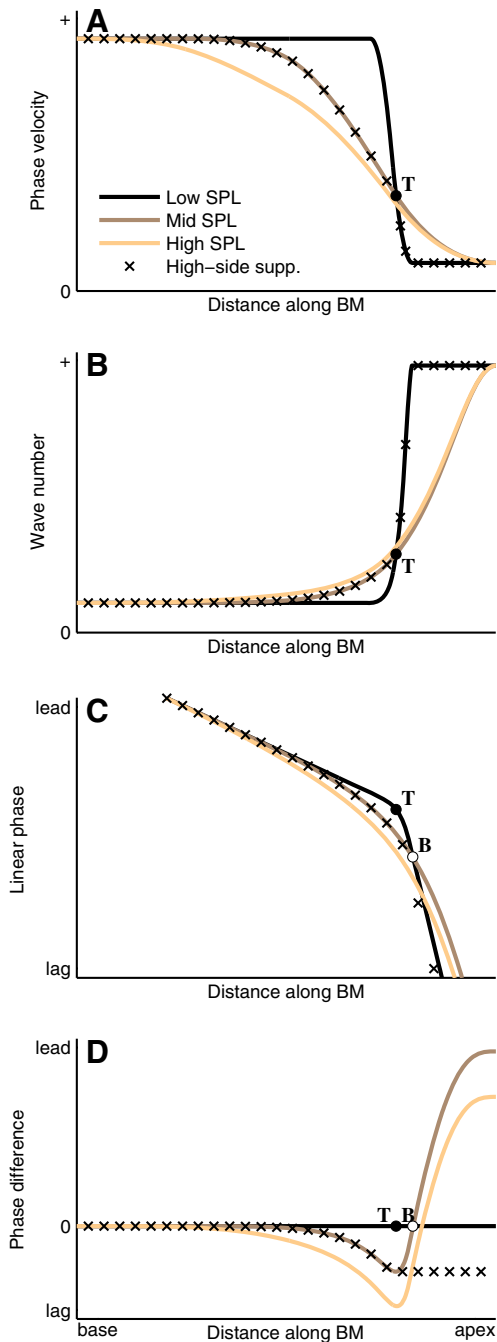


FIG. 16. The effect of suppression on wave velocity and phase. **A** Velocity profiles of traveling waves subject to varying levels of suppression. The low-intensity reference (*black curve*), shows a rapid transition (marked T) from the fast basal portion of the wave to the slow apical portion. Increasing amounts of suppression cause a progressive smoothing of the transition (*brown and ochre lines*), causing a pivoting around T (see text). The \times s mark the effect of a high-side suppressor having a spatial range that is restricted to locations basal to T. **B** The corresponding wave number profiles show a transition from small to large values and a suppression-induced pivoting. **C** The local phase, obtained from spatial integration of wave number. The unsuppressed wave (*black curve*) shows the transition as a sharp kink, which is rounded by suppression (see text). The point B at which the phase is unaffected by mid-level suppressors lies apical to T. **D** Suppressor-induced phase shifts obtained by using the unsuppressed phase profile of panel C as a reference.

From Figure 16D, the phase leads at the apical end of the wave are predicted to depend nonmonotonically on suppressor intensity. This prediction is correct, as shown by the nonmonotonicities above CF in Figure 7B, D. Interestingly, this nonmonotonic dependence on intensity does not originate from any reversals in the effect of suppressor intensity on local wave velocity (see Fig. 16A), but from a competition between the slowing down and speeding up in subsequent stages of the travel path.

High-side suppressors only partially overlap with the probe wave (Fig. 12C), and this biases the way they affect probe phase. The basal portion of the probe wave is affected, but the apical portion will often be beyond the reach of the suppressor. Thus, the basal slowing down is not (as much) followed by an apical speeding up, as was the case for low-side suppressors. This explains why high-side suppressors primarily cause phase lags (Figs. 7F and 8D). The \times s in Figure 16 illustrate the effects of a high-side suppressor whose dominance extends only to the pivot point T. Once the probe wave has traveled past T, its velocity is not affected anymore. The phase lag accumulated up to this point, however, is not undone either, and the phase shift becomes constant (*black \times symbols* branching off the *brown curve* in Figure 16D).

Propagation speed and multilocation recordings

The intensity-induced changes in propagation velocity that we inferred from recorded phase shifts were actually reported by Ren et al. (2011), who compared pure-tone responses between two adjacent reflective beads on the BM. Their Figures 2D and 3D show a pivoting of phase velocity: with increasing intensity, phase velocity decreased/increased below/above a pivot frequency. The pivot frequency was lower than the CFs of the beads. This corresponds (via scaling) to the pivot *location* T being basal to the wave's best site B (Fig. 16). The velocity curves of Ren et al. also show that, with increasing intensity, the speeding up at high frequencies saturates, whereas the slowing down at low frequencies continues. This corresponds (via scaling) to the saturation of high-intensity changes in the basal portion of the velocity profile in Figure 16A. The intensity-induced velocity changes of Ren et al. amount to a factor ~ 0.5 (low-frequency slowing down) and ~ 1.5 (high-frequency speeding up).

It is not feasible to estimate the changes in wave velocity underlying the phase shifts in our data, because scaling arguments have limited validity. While it is reasonable to assume that the effects of moving the recording location along the BM are roughly similar to scaling the stimulus frequencies (because of the frequency-place map), such a tradeoff is not necessarily quantitatively exact. In fact, multilocation BM data (e.g., Ren 2002) show considerable violations of the type of

mathematical “scaling invariance” proposed by Zweig (1976). One might attempt to refine the scaling prescription, but such semitheoretical speculations can never replace real data. An obvious suggestion for future work is therefore to perform two-bead BM recordings and directly measure the effect of suppressors on the propagation velocity of the probe wave.

The spatial onset of suppression and phase shifts; antisuppression

We estimated the spatial extent of the suppressible portion of the probe wave by converting the values of $f_{\min, \text{Amp}}$ (the lowest probe frequencies at which suppression was observed; Fig. 2) to distances on the BM using the frequency place map of the gerbil (Müller 1996). Suppressible amplitude effects were found to start building up $730 \pm 120 \mu\text{m}$ ($N=5$) basal to the best site of the wave, comparable to the $\sim 1\text{-mm}$ long region basal to the peak contributing to compression as estimated from pure-tone responses in various BM studies (reviewed in Robles and Ruggero 2001). Intriguingly, the spatial onset of suppressor-induced *phase* shifts (obtained in the same way) was more basal, amounting to $1,350 \pm 350 \mu\text{m}$ ($N=5$) basal to the best site of the wave. Systematic phase effects appear to precede systematic amplitude suppression. The spatial onset of nonlinear phase effects coincides with the region of antisuppression (where the probe response is *enhanced* by a high-intensity suppressor). The phase-versus-amplitude plots (Fig. 8) further illustrate the relation between phase and amplitude effects near the spatial onset of suppression. The antisuppression effects near $f_{\text{probe}} = \text{CF}/2$ are small but systematic, and consistent across animals. Antisuppression of below-CF probes is also visible in Figure 4B of Rhode (2007b), but was not discussed in that study. Antisuppression is closely related to expansive growth of below-CF responses found by Cooper (2000a), Rhode (2007a), and Versteegh and Van der Heijden (2012); the latter study discusses a possible explanation in terms of intensity-induced changes of BM stiffness suggested by Allen (1980).

The complex case of single tones

Single-tone BM responses combine the roles of suppressor and probe in a single component, and this sets up a chain of self-interaction in which the BM displacement in one longitudinal segment controls the propagation, which in turn determines the displacement in the next segment, etc. It is difficult to derive the spatial envelope of the wave from recordings obtained at a single location. Scaling arguments are based on the assumption that the propagation properties of the cochlea are uniform. In reality, tonal stimulation disturbs any uniformity by evoking a strongly localized BM displace-

ment, and this pattern of disturbance will shift with the frequency of the tone. Thus, the relation between local BM vibration at different frequencies (the data) and the spatial profile of single waves (the construction) hinges on a mix of frequency selectivity and nonlinear properties that cannot be disentangled without additional data (e.g., wideband responses) or specific model assumptions (De Boer and Nuttall 2002). Pure-tone BM responses are therefore much harder to analyze and interpret than wideband responses. Nevertheless, the major differences between the nonlinear effects evoked by single tones on the one hand, and tone pairs and wideband stimuli on the other, can be understood without much quantitative detail.

At the apical end of a traveling wave (beyond the peak), the magnitude of BM displacement decays rapidly, rendering this part of the wave a poor suppressor of anything—including itself. Thus, the self-suppression observed beyond the peak is primarily inherited from more basal locations. (In that respect, self-suppression of single tones resembles high-side suppression; Figures 12C and 14A). Even though the decaying portion of the wave is a poor *suppressor*, as a *probe* it is very sensitive to the nonlinear effects of local increments in BM displacement (Fig. 10E). It therefore takes a division of labor—an above-CF probe plus a lower-frequency suppressor—to fully expose the strong suppressive effects inflicted on the decaying portion of the traveling wave.

From these considerations, one expects above-CF nonlinearities to be weaker in single-tone responses than in wideband responses. Indeed, the comparison between single-tone and wideband BM responses in Fig. 6 of Versteegh and van der Heijden (2012) shows the expected contrast in the nonlinear effects of intensity on both amplitude and phase, and it was exactly this above-CF contrast that caused systematic errors in their attempts to predict one type of response from the other (their Fig. 7). Perhaps the most dramatic illustration of the contrast between single tones and wideband responses is found in the phase shifts. Intensity-induced phase shifts in single-tone responses rarely exceed 0.25 cycle, even at intensities exceeding 90 dB SPL (Robles and Ruggero 2001; Rhode 2007a; Versteegh and Van der Heijden 2012). In comparison, suppression of above-CF probes by mid-intensity suppressors yields much larger phase shifts ranging from ~ 0.5 cycle (Rhode 2007a; Versteegh and Van der Heijden 2012) to >1 cycle (Fig. 6).

From the abundant single-tone BM data in the literature, one could easily perceive intensity-induced phase shifts to be secondary or marginal compared to the changes in sensitivity. In fact, they can be quite substantial for wideband stimuli at moderate intensities (Fig. 6). The large phase shifts and the underlying changes in phase velocity (Ren et al. 2011) present a

challenge to the modeling of traveling waves in the cochlea. Phase velocity primarily depends on stiffness and mass, whereas damping has only a second-order effect (Whitham 1974). Accordingly, intensity-induced phase shifts are small in the common type of cochlear models that incorporate nonlinearity by variable damping of the cochlear partition (De Boer and Viergever 1982). The large size of the phase effects and their earlier spatial onset may point to a fundamental role of variable propagation speed as a means of controlling the wave amplitude.

CONCLUSION

Many aspects of suppression on the BM, including:

- dependence on probe frequency and suppressor frequency
- rate of growth with suppressor intensity
- large contrast between low-side and high-side suppression
- complex mix of phase leads and lags

appear at a first glance to be a set of disparate phenomena. Yet they become logically connected once viewed in the framework of propagating waves and the spatial buildup of suppressive effects along the propagation direction. This perspective on cochlear nonlinearity affords a unification of compressive and suppressive effects anticipated by empirical (Cooper 1996) and theoretical (Kanis and De Boer 1993) studies.

Specifically, the local propagation of any component is strongly controlled by the local displacement magnitude of the BM, which is in turn determined by all the components traveling at the location. Local changes in displacement magnitude affect both the *efficiency* and the *speed* of local wave propagation, thereby creating measurable changes in amplitude and phase, respectively.

Although the mechanisms behind the local effects cannot be inferred from the data, the same mechanisms appear to be at work for low-side suppression, high-side suppression, and overall intensity increments of single tones or wideband stimuli. The widely different manifestation of cochlear nonlinearity in these cases can be understood from differences in spatial distribution of the same local effects. The traveling wave character of BM motion is the foundation of this unified description of cochlear nonlinearity. Vibrations at each point are passed to the next point. It is this unidirectional propagation that shapes the spatial buildup of nonlinear effects.

Compressive growth of BM responses is often explained in terms of variable damping in a restricted region basal to the peak of the traveling wave. Several

of our findings indicate that this view of cochlear nonlinearity is incomplete or oversimplified:

- the anti-suppression at the spatial onset of nonlinearity
- the dominance of phase effects (rather than amplitude effects) near the spatial onset of nonlinearity
- the very large (>1 cycle) suppressor-induced phase shifts
- the continued accumulation of suppressive effects beyond the peak of the probe wave.

A true understanding of cochlear nonlinearity requires a perfect disentanglement of spatial effects and the effects of stimulus frequency. Eventually, arguments based on scaling must be replaced by direct spatial measurement. In our view, the most promising approach is to study suppression using multilocation recordings.

ACKNOWLEDGMENTS

The authors thank Nigel Cooper, Wei Dong, Lisa Olson, and Alberto Recio for their generous help with setting up the measurements. This work is supported by Netherlands Organization for Scientific Research (NWO) grants 818.02.007 and 834.10.005 (Earth and Life Sciences).

Open Access This article is distributed under the terms of the Creative Commons Attribution License which permits any use, distribution, and reproduction in any medium, provided the original author(s) and the source are credited.

REFERENCES

- ALLEN JB (1980) Cochlear micromechanics—a physical model of transduction. *J Acoust Soc Am* 68:1660–1670
- ANDERSON DJ, ROSE JE, HIND JE, BRUGGE JF (1971) Temporal position of discharges in single auditory nerve fibers within the cycle of a sine-wave stimulus: frequency and intensity effects. *J Acoust Soc Am* 49:1131–1139
- CHEATHAM MA (2008) Comment on "Mutual suppression in the 6 kHz region of sensitive chinchilla cochlea" [*J. Acoust. Soc. Am.* 121, 2805–2818 (2007)]. *J Acoust Soc Am* 123:602–605
- COOPER NP (1996) Two-tone suppression in cochlear mechanics. *J Acoust Soc Am* 99:3087–3098
- COOPER NP (2000A) Basilar membrane vibrations in the basal turn of the gerbil cochlea. The Twenty-third Midwinter Research Meeting of Association for Research in Otolaryngology, St. Petersburg Beach, FL, USA
- COOPER NP (2004) Compression in the peripheral auditory system. In: Bacon SP, Fay RR, Popper AN (eds) *Compression: from cochlea to cochlear implants*. Springer, New York, pp 18–61
- COOPER NP (2000B) Radial variation in the vibrations of the cochlear partition. In: Wada H, Takasaka T, Ikeda K, Ohyama K, Koike T (eds) *Recent developments in auditory mechanics*. World Scientific, Singapore, pp 109–115
- COOPER NP, RHODE WS (1996) Two-tone suppression in apical cochlear mechanics. *Aud Neurosci* 3:123–134
- DE BOER E, NUTTALL AL (2002) The mechanical waveform of the basilar membrane. IV. Tone and noise stimuli. *J Acoust Soc Am* 111:979–989

- DE BOER E, VIERGEVER MA (1982) Validity of the Liouville–Green (or WKB) method for cochlear mechanics. *Hear Res* 8:131–155
- DELGUTTE B (1990) Physiological mechanisms of psychophysical masking: observations from auditory-nerve fibers. *J Acoust Soc Am* 87:791–809
- GEISLER CD, NUTTALL AL (1997) Two-tone suppression of basilar membrane vibrations in the base of the guinea pig cochlea using "low-side" suppressors. *J Acoust Soc Am* 102:430–440
- GEISLER CD, YATES GK, PATUZZI RB, JOHNSTONE BM (1990) Saturation of outer hair cell receptor currents causes two-tone suppression. *Hear Res* 44:241–256
- KANIS LJ, DE BOER E (1993) Self-suppression in a locally active nonlinear model of the cochlea: a quasilinear approach. *J Acoust Soc Am* 94:3199–3206
- KIM DO, MOLNAR CE, MATTHEWS JW (1980) Cochlear mechanics: nonlinear behavior in two-tone responses as reflected in cochlear-nerve-fiber responses and in ear-canal sound pressure. *J Acoust Soc Am* 67:1704–1721
- KIM DO, MOLNAR CE, PFEIFFER RR (1973) A system of nonlinear differential equations modeling basilar-membrane motion. *J Acoust Soc Am* 54:1517–1529
- MØLLER AR (1965) An experimental study of the acoustic impedance of the middle ear and its transmission properties. *Acta Otolaryngol (Stockh)* 60:129–149
- MÜLLER M (1996) The cochlear place-frequency map of the adult and developing mongolian gerbil. *Hear Res* 94:148–156
- NUTTALL AL, DOLAN DF (1993) Two-tone suppression of inner hair cell and basilar membrane responses in the guinea pig. *J Acoust Soc Am* 93:390–400
- PALMER A, SHACKLETON T (2009) Variation in the phase of response to low-frequency pure tones in the guinea pig auditory nerve as functions of stimulus level and frequency. *J Assoc Res Otolaryngol* 10:233–250
- PATUZZI R, SELICK PM, JOHNSTONE BM (1984) The modulation of the sensitivity of the mammalian cochlea by low frequency tones. III. Basilar membrane motion. *Hear Res* 13:19–27
- REN T (2002) Longitudinal pattern of basilar membrane vibration in the sensitive cochlea. *Proc Natl Acad Sci U S A* 99:17101–17106
- REN T, HE W, PORSOV E (2011) Localization of the cochlear amplifier in living sensitive ears. *PLoS One* 6:e20149
- RHODE WS (2007A) Basilar membrane mechanics in the 6–9 kHz region of sensitive chinchilla cochleae. *J Acoust Soc Am* 121:2792–2804
- RHODE WS (2007B) Mutual suppression in the 6 kHz region of sensitive chinchilla cochleae. *J Acoust Soc Am* 121:2805–2818
- RHODE WS, COOPER NP (1993) Two-tone suppression and distortion production on the basilar membrane in the hook region of cat and guinea pig cochleae. *Hear Res* 66:31–45
- RHODE WS, RECIO A (2001A) Basilar-membrane response to multicomponent stimuli in chinchilla. *J Acoust Soc Am* 110:981–994
- RHODE WS, RECIO A (2001B) Multicomponent stimulus interactions observed in basilar-membrane vibration in the basal region of the chinchilla cochlea. *J Acoust Soc Am* 110:3140–3154
- ROBLES L, RUGGERO MA (2001) Mechanics of the mammalian cochlea. *Physiol Rev* 81:1305–1352
- ROSOWSKI JJ, RAVICZ ME, SONGER JE (2006) Structures that contribute to middle-ear admittance in chinchilla. *J Comp Physiol A Neuroethol Sens Neural Behav Physiol* 192:1287–1311
- RUGGERO MA, ROBLES L, RICH NC (1992) Two-tone suppression in the basilar membrane of the cochlea: mechanical basis of auditory-nerve rate suppression. *J Neurophysiol* 68:1087–1099
- SACHS MB, KIANG NY (1968) Two-tone inhibition in auditory-nerve fibers. *J Acoust Soc Am* 43:1120–1128
- SHERA CA (2007) Laser amplification with a twist: traveling-wave propagation and gain functions from throughout the cochlea. *J Acoust Soc Am* 122:2738–2758
- TEMCHIN AN, RECIO-SPINOSO A, CAI H, RUGGERO MA (2012) Traveling waves on the organ of Corti of the chinchilla cochlea: spatial trajectories of inner hair cell depolarization inferred from responses of auditory-nerve fibers. *J Neurosci* 32:10522–10529
- VAN DER HEIJDEN M, JORIS PX (2006) Panoramic measurements of the apex of the cochlea. *J Neurosci* 26:11462–11473
- VERSTEEGH C, VAN DER HEIJDEN M (2012) Basilar membrane responses to tones and tone complexes: nonlinear effects of stimulus intensity. *J Assoc Res Otolaryngol* 13:785–798
- WEGEL RL, LANE CE (1924) The auditory masking of one pure tone by another and its probable relation to the dynamics of the inner ear. *Physical Review* 23:266–285
- WHITHAM GB (1974) *Linear and nonlinear waves*. Wiley, New York
- ZWEIG G (1976) Basilar membrane motion. *Cold Spring Harb Symp Quant Biol* 40:619–633